HHS Public Access

Author manuscript

J Immunol. Author manuscript; available in PMC 2018 November 01.

Published in final edited form as:

J Immunol. 2017 November 01; 199(9): 3158–3175. doi:10.4049/jimmunol.1700475.

H3K27 methylation dynamics during CD4 T cell activation: regulation of JAK/STAT and IL12RB2 expression by JMJD3

Sarah A. LaMere[1,†,*], **Ryan C. Thompson**[1], **Xiangzhi Meng**[1], **H. Kiyomi Komori**[1,‡], **Adam Mark**[1,§], and **Daniel R. Salomon**[1]

[1]Department of Molecular & Experimental Medicine, The Scripps Research Institute, La Jolla, California, USA

Abstract

The changes to the epigenetic landscape in response to antigen during CD4 T cell activation have not been well characterized. While CD4 T cell subsets have been mapped globally for numerous epigenetic marks, little has been done to study their dynamics early after activation. We have studied changes to promoter H3K27me3 during activation of human naïve and memory CD4 T cells. Our results show that these changes occur relatively early (1 day) after activation of both naïve and memory cells, and that demethylation is the predominant change to H3K27me3 at this time point, reinforcing high expression of target genes. Additionally, inhibition of the H3K27 demethylase, JMJD3, in naïve CD4 T cells demonstrates how critically important molecules required for T cell differentiation, such as JAK2 and IL12RB2, are regulated by H3K27me3. Our results demonstrate that H3K27me3 is a dynamic and important epigenetic modification during CD4 T cell activation, and that JMJD3-driven H3K27 demethylation is critical for CD4 T cell function.

Keywords

H3K27 methylation; epigenetics; CD4 T cell activation; immune memory; ChIP-seq; JMJD3

Introduction

CD4 T cells are an integral component of the adaptive immune response, facilitating antigen-specific ‘memory’ via adaptation following exposure to pathogens and other foreign invaders. The molecular mechanisms responsible for the transition to memory are still poorly understood and likely stem from multiple epigenetic processes in the cell following activation (1). Numerous epigenetic marks have been explored in both cancer and embryonic stem (ES) cell differentiation, including DNA methylation, histone modifications, and chromatin regulators, all of which appear to play roles in modulating gene expression (2–5).

[*]Corresponding Author: Sarah LaMere, D.V.M., Ph.D., Department of Pathology, University of California San Diego, 9500 Gilman Dr., La Jolla, CA 92093, Phone: (858) 947-5055, salamere@ucsd.edu.
[†]Department of Pathology, University of California San Diego, La Jolla, California, USA
[‡]Synthetic Genomics, La Jolla, California, USA
[§]Avera McKennan Hospital & University Health Center, La Jolla, California, USA

GEO accession # GSE73214 (https://www.ncbi.nlm.nih.gov/geo/query/acc.cgi?acc=GSE73214)

These marks can target multiple regulatory regions, including promoters, enhancers, super-enhancers, gene bodies, and intergenic regions, which confer another layer of complexity to this already enigmatic system. Epigenetic studies in T cells have been more limited, and in this early phase of investigation are still largely descriptive, although clear correlations between epigenetic modifications and T cell differentiation have been illustrated with genome-wide studies (6–13).

H3K27me3 in particular is a conventionally ‘repressive’ histone modification (9, 14) that plays a role in CD4 T cell differentiation (15, 16). However, its dynamics during CD4 T cell activation and early differentiation have not been explored, and its role in early differentiation is still poorly characterized. One study performed global mapping of H3K27me3 after *in vitro* polarization of murine CD4 T cell differentiation to reveal that the presence of H3K27me3 in Th-related genes corresponded to silencing of those genes in their opposing lineages (7). A study of murine CD8 T cell dynamics after viral infection also demonstrated a profound loss of H3K27me3 following activation, supporting the role of repressive H3K27me3 marks in naïve CD8 T cells to maintain a state of restraint during rest (8).

Two demethylases, JMJD3 and UTX, are known to catalyze H3K27me3 demethylation. Recently an exploration into the role of Jmjd3 in mice upon the regulation of CD4 T cell differentiation found that a conditional knock-out of Jmjd3 resulted in skewing to Th2 and Th17 differentiation (15). Both demethylases are required for *in vivo* thymocyte differentiation in mice (17). In ES cells, JMJD3 appears to delocalize PRC proteins, which is essential for further development. Additionally, UTX is a component of the MLL complex, strongly suggesting that H3K27 demethylation can be coupled with the “activating” methylation of H3K4 by MLL (18). UTX is ubiquitously expressed in tissues and is also important for embryonic cell development (19). In contrast, JMJD3 is commonly induced during inflammation or upon exposure to antigenic or oncogenic stimuli (18, 20, 21). JMJD3 inhibits somatic cell reprogramming in inducible pluripotent stem cells (iPS), while UTX is essential for it, suggesting contrasting roles for these two enzymes (22, 23). The two enzymes also play contrasting roles in acute lymphoblastic leukemia (ALL), with JMJD3 inducing the neoplastic process and UTX acting as a tumor suppressor (24).

In the current study we have examined the dynamics of promoter-associated H3K27me3 upon activation of human naïve and memory CD4 T cells. We find that in both subsets, profound demethylation of H3K27 is observed by 1 day after activation, which is in contrast to H3K4 methylation, where changes are not observed until days later (25). Mapping specific states of H3K27me3 to known immune pathways demonstrates that loss of H3K27me3 early in activation corresponds to pathways crucial to T cell function, including T cell activation and the JAK-STAT pathways. Mechanistic studies by perturbation of H3K27 demethylation with a small molecule inhibitor (GSK-J4) and siRNA knockdown of the two H3K27 demethylases confirms that H3K27 demethylation by JMJD3 is important for key members of early differentiation-related pathways. Altogether, these data confirm that H3K27 is a highly dynamic epigenetic modification in CD4 T cells during early activation, and the nature of these dynamic changes is crucial to CD4 T cell function.

Materials and Methods

Ethics Statement

All the studies in this manuscript were covered by Human Subjects Research Protocols approved by the Institutional Review Board of The Scripps Research Institute. Informed written consent was obtained from all study subjects in the study.

Isolation and activation of human lymphocytes

Peripheral blood was collected from healthy donors, and peripheral blood mononuclear cells (PBMC) were collected by centrifugation through a histopaque (Sigma) gradient. CD4 T cells were negatively selected using the EasySep™ Human Naive CD4+ T or Memory CD4 T Cell Enrichment Kits (Stemcell Technologies) from 4 donors. Cell purity was assessed by flow cytometry with antibodies specific for CD4, CD45RA, CD45RO (SK3, HI100, UCHL1, eBioscience). Data acquisition was conducted on an LSR-II (BD Biosciences) and analysis was performed using FlowJo (Treestar). Live cells were gated based on forward by side scatter area, and doublets were excluded based on forward scatter height by forward scatter width and side scatter height by side scatter width. Live cells were then gated on CD4 staining and cell purity following isolation was determined by CD45RA vs. CD45RO staining. Cell purity for all donors was >94%.

CD4 T cells were cultured in RPMI 1640 (Mediatech) supplemented with 100 U/ml Penicillin, 100 μg/ml Streptomycin and 10% FBS at 37° C and 5% CO_2. T cells were activated with DynaBead Human T-Activator CD3/CD28 (Invitrogen) for 1 and 5 days. Cells maintained in culture out to 2 weeks received 30 U/mL of human recombinant IL-2 every 2 days. (NIH repository) beginning at day 5 after activation. Samples for ChIP-seq and RNA-seq were collected from the 4 donors at rest, 1 day, 5 days, and 2 weeks after activation. GSK-J4 experiments were conducted with a 24 h incubation in 12.5 uM GSK-J4 in 0.2% DMSO alongside a 0.2% DMSO vehicle control prior to activation. T cells were activated with DynaBead Human T-Activator CD3/CD28 (Invitrogen) for 8 and 24 h and collected for quantitative RT-PCR, ChIP-qPCR, and flow cytometry as described below. For IL-6 rescue experiments, 20 ng/mL of recombinant human IL-6 (Tonbo Biosciences) resuspended in PBS was added to media at the time of activation, while an equal volume of PBS (2 uL/mL) was added to the control.

Chromatin Immunoprecipitation for H3K27me3

3×10^7 cells were fixed for 10 min in cell culture medium with 1% formaldehyde at room temperature. Fixation was quenched with 10% glycine for 5 min at room temperature. Cell pellets were flash frozen in liquid nitrogen and stored at −80 °C until chromatin isolation. Chromatin was isolated from cell pellets using the ChIP-It Express Enzymatic Shearing Kit (Active Motif) per the manufacturer's instructions. For immunoprecipitation, 7.5 μg of chromatin was diluted in a total of 1 mL of low salt wash buffer (0.1% SDS, 1.0% Triton X-100, 2 mM EDTA, 20 mM Tris-HCl (pH 8.1), 500 mM NaCl) with protease inhibitor cocktail and pre-cleared with 30 μL of Invitrogen Dynal Protein G magnetic beads for 2 h at room temperature with rotation. 20 μL of pre-cleared chromatin was saved for input analysis and stored at −80 °C. Remaining chromatin was incubated with 2 μL of anti-H3K27me3

antibody (Millipore, catalog #17-622) overnight at 4°C with rotation. 30 μL of Invitrogen Dynal Protein G beads were added to each ChIP and incubated at 4 °C with rotation for 2 h. Beads were washed three times in low salt wash buffer and then two times with high salt wash buffer (0.1% SDS, 1.0% Triton X-100, 2 mM EDTA, 20 mM Tris-HCl (pH 8.1), 500 mM NaCl) with 5 min of rotation at 4 °C for each wash. Beads were resuspended in 150 μL of elution buffer (1% SDS, 0.1M $NaHCO_3$) and incubated in a thermomixer at 65 °C for 30 minutes at 1,200 rpm to reverse cross-linking. 2 μL of Proteinase K (Invitrogen) was added to each sample, and 6 μL of 5 M NaCl was added for a total concentration of 200 mM. Samples were then incubated in a thermomixer at 65 °C overnight at 1,200 rpm. Eluted samples were removed from the beads and purified using the Qiagen Qiaquick PCR purification kit per the manufacturer's instructions.

Preparation of sequencing libraries for ChIP-seq and deep RNA sequencing

RNA for RNA-seq was isolated from purified cells using an All Prep kit (QIAGEN) following the manufacturer's instructions, and purified total RNA was converted to cDNA using Ovation RNA-seq (NuGEN) followed by S1 endonuclease digestion (Promega) as previously described (26). Digested cDNA libraries were then end-repaired and A-tailed. Indexed adapters were ligated, and ligation product was purified on Agencourt AMPure XP beads (Beckman Coulter Genomics) followed by size selection from 2% agarose. Purified product was amplified with 15 cycles of PCR followed by size selection from 2% agarose. Libraries were assessed on an Agilent Bioanalyzer using a DNA chip and quantitated using the Quant-iT ds DNA BR Assay kit (Invitrogen) and a Qubit Fluorimeter (Invitrogen). Cluster generation and sequencing of 100 bp single-end reads on an Illumina HiSeq 2000 system was conducted with purified libraries following manufacturer's instructions. Depth of sequencing per sample was 15 million aligned reads.

For ChIP-seq, 10 ng of purified DNA from individual chromatin IPs were end repaired and A-tailed. Indexed adapters were ligated, and ligation product was purified on Agencourt Ampure XP beads and processed using Illumina DNA TruSeq protocols.

Chromatin Immunoprecipitation for JMJD3

For JMJD3 ChIP-seq, 3 million naïve CD4 T cells were fixed by re-suspending in 1 mL of culture medium and cross-linking with 100 μL of fixation buffer (High Sensitivity ChIP kit, Active Motif) at room temperature for 15 minutes. 55 ul of stop solution was added to quench unreacted formaldehyde and incubated at room temperature for 10 minutes. Fixed cells were centrifuged at 700 × g at 4°C for 10 minutes and washed with 5 mL of cold PBS. After aspirating the supernatants, fixed pellets were stored at −80°C. Prior to chromatin preparation, pellets were thawed on ice and resuspended in 1 ml ice-cold Lysis Buffer supplemented with 5 μl PIC + 5 μl PMSF (ChIP-It Express Enzymatic Shearing Kit, Active Motif). Pellets were incubated on ice for 30 minutes and then centrifuged at 5000 rpm for 10 min at 4°C. Pelleted nuclei were re-suspended in 130 ul of ice-cold shearing buffer (10mM Tris PH8.1 + 0.1% SDS + 1mM EDTA) and transferred into a Covaris microTube. Chromatin was sheared into 200 bp (5% duty, Intensity:4, 200cycle/burst, 30s/cycle for 30min, 4°C). Sheared chromatin was centrifuged at max speed for 10 min at 4°C. Newly prepared chromatin was transferred to a new tube and re-suspended in 250 uL of PBS with

1ul of PIC. Chromatin was pre-cleared with 10 uL of protein G beads and rotated for 2 hours at 4°C. Pre-cleared chromatin samples were incubated with 2 ug of anti-JMJD3 antibody (ab38113, Abcam), rotating overnight at 4°C, and immunoprecipitation was performed as for H3K27me3 ChIP.

RNA-seq of JMJD3 siRNA knockdowns

Human naïve CD4 T cells were transfected by electroporation with 2 uM JMJD3 specific siRNA (ON-TARGETplus siRNA smartpool, GE Dharmacon) or scrambled siRNA controls. Cells were then activated with anti-CD3/CD28 beads at 10 ul per million cells 24 h after transfection, and then cells were collected 24 h after activation. Total RNA from 5 million of either siJMJD3 or scramble control cells of 4 donors were isolated by RNeasy Plus Mini Kit (74136, Qiagen), and quantified by Qubit. 25 ng of total RNA of each sample was used as input for library preparation by Ion AmpliSeq Transcriptome Human Gene Expression Kit (Life technologies, A26325). Barcoded libraries were multiplexed and templated on Ion Chef system and then sequenced on the Ion Proton using the Ion AmpliSeq Transcriptome Human Gene Expression Panel.

ChIP-seq analysis

Reads were aligned to hg19 using bowtie2 (27). Sample normalization factors adjusting for sequencing depth and compositional bias for each histone mark were determined by un-weighted Trimmed Mean of M-values (TMM) on 10 kb bin read counts (28). These normalization factors were used in all differential binding analyses described below. For each condition, peaks were called independently for each of the four donors using the MACS peak caller on the aligned reads. Then biologically reproducible consensus peaks were determined using the Irreproducible Discovery Rate framework with a threshold of 0.01. The same process was repeated with all aligned reads from all conditions to obtain a single set of condition-independent consensus peaks for cross-condition comparison. This procedure was repeated for H3K27me3 and H3K4me3 samples to obtain condition-specific and condition-independent peak sets for both histone marks. For each histone mark, reads whose 5-prime mapping location overlapped each condition-independent consensus peak were counted for each sample. Counts were analyzed for differential binding between conditions using edgeR’s quasi-likelihood F-test (29), with a model including the condition as the main effect and donor as a batch effect. P-values were adjusted for multiple testing using the method of Benjamini & Hochberg (30). Sliding-window based differential binding analysis was performed (28) using the same model as for the peak analysis. In each comparison, windows were only included in the analysis for that comparison if they had a mean log CPM of −1 or more across all samples in that comparison.

In order to determine the effective promoter radius for each histone mark, the distance from each unique TSS annotated in the UCSC gene database to the distance to the nearest peak was determined for each condition’s consensus peak set. The distribution of these distances was plotted. It was assumed that these histone marks would be uniformly distributed throughout most of the genome, but enriched in promoters. For all histone marks and conditions, visual inspection revealed a peak at small distances and flat background level at larger distances, consistent with the assumption of enrichment of peaks near promoters. For

H3K27me3, the distribution flattens out to the background level near 2.5 kb. These distances were used as the effective promoter radius when defining the promoter region associated with each transcriptional start site (TSS). The promoter region of each annotated transcript was defined by extending a region upstream and downstream from the TSS by the determined radius. Overlapping promoters from the same gene were merged into one. The number of reads overlapping each promoter in each sample was counted. Promoter counts were analyzed using the same model as for the peak analysis. As a negative control, the ChIP-seq input samples were also analyzed in the same way to verify that the differential binding test did not give false positive results.

Because dispersions were found to vary with time point, each test for differential binding between conditions was conducted using dispersions estimated from only the samples from time points associated with the conditions being tested. For example, for comparing memory at rest vs. memory 5 days after activation, all samples from rest and 5 days were used for estimating dispersions. Results for differential binding were filtered with an FDR cut-off of 0.1 and a fold enrichment cut-off of $\log_2$ fold change >1 or <−1.

Analysis by enrichment or peaks

As described for the ChIP-seq analysis, differential binding was calculated when comparing samples across time points, allowing for evaluation of changes in overall enrichment. This type of analysis is a powerful adjunct to the analysis of peaks because it allows for examination of histone modification changes outside of called peaks within a larger sequence frame and has been used in other studies (31–33). Within the 5 kb radius around the promoter that we examined (i.e. 2.5 kb up- and downstream), peaks might be called in two or more conditions, but calculations for differential binding still suggest there is differential enrichment. Therefore, we have used both types of analyses in this study when comparing different conditions – one comparison in which a quantitative difference in enrichment is calculated, and another in which qualitative comparisons are made for the presence or absence of peaks within the promoter radius.

RNA-seq analysis

RNA-seq reads were aligned to the UCSC hg19 transcriptome and genome using Tophat 2 (34). The number of reads aligning unambiguously to each gene in each sample was computed. Genes without at least 5 reads assigned in at least one sample were considered not detected and were discarded. Normalization factors were computed using TMM, and these normalization factors were used for differential expression analysis and quantification. Gene counts were analyzed for differential expression using the same model as for the peak analysis. Gene expression levels for each sample were quantified as FPKM (fragments per kilobase per million fragments sequenced), using the length of the longest transcript isoform for each gene. Batch-corrected average gene expression levels for each condition were quantified by back-transforming the fitted model coefficients for each condition onto a raw count scale and then normalizing to FPKM as for the sample counts. Cut-offs imposed for differential expression analysis included an FDR of <0.05 and $\log_2$ fold change of +/−1.

ChIP-seq and RNA-seq combined analysis

Tests were performed for correlation between presence of a ChIP-seq peak at a given experimental condition and either RNA-seq expression level (FPKM values) at a given experimental condition or expression $\log_2$-fold change between two conditions, for all genes in the genome. First, genes were partitioned by promoter peak presence or absence, and then a Kolmogorov-Smirnoff test (a non-parametric test for distributional differences) was performed to test for significant differences in the RNA-seq statistic of interest between the partitions, and 95% confidence intervals for the difference in means were constructed (based on an assumption of a normal distribution).

Pathway analysis

Functional pathway mapping was conducted using Ingenuity Pathway Analysis (IPA, QIAGEN, www.qiagen.com/ingenuity) and included p-values and log fold changes for differential enrichment or differential expression where appropriate. Pathway mapping in parallel using ImmuneMap, Panther, and Gene Ontology (GO) supplemented the final pathway results.

RNA isolation and cDNA synthesis for qRT-PCR

Cells harvested for RNA (5×10^6 cells) were washed 3 times in 1 mL of phosphate buffered saline (PBS) without calcium and magnesium (Corning), flash frozen in liquid nitrogen, and stored at −80° C until RNA purification. Total RNA was isolated using RNeasy Mini Kit (Qiagen) and RNA concentration was determined by nanodrop. First-strand cDNA was synthesized from 500ng RNA in a 20 uL reaction volume using the BioRad iScript system (Bio-Rad Laboratories). The complete reaction mix was incubated for 5 minutes at 25°C, 30 minutes at 42°C and 5 minutes at 85°C. The synthesized cDNA was stored at −20°C for further qPCR analysis.

Quantitative PCR

For qRT-PCR, synthesized cDNA was mixed with PerfeCTa® SYBR® Green SuperMix (Quanta BioSciences), and one of the primer sets. Reactions were performed on a HT7900 Fast-realtime PCR System (Applied Biosystems) under optimized cycling conditions consisting of a 10-minute initial denaturing step at 95°C, followed by up to 40 cycles of amplification (denaturation at 95°C for 10 seconds, annealing and extension at 60°C for 30 seconds). Then a melting curve was measured from 65°C to 98°C. The specificity of each of the PCR products was confirmed a narrow peak appeared in the melting curve when temperature rose above 72°C. The expression level of each gene was evaluated relative to beta-2 microglobulin (B2M) using the 2(-Delta Delta C(T)) method (35). For ChIP-qPCR, 2 uL of purified DNA from H3K27me3 ChIP or 2% input samples from each condition were subjected to qPCR using the same protocol as for cDNA, and percent input was calculated using the equation $100 \times 2^{Ct(input) - Ct(IP)}$. Primer sequences included the following: JAK2 (F-TCTGGGGAGTATGTTGCAGAA, R-AGACATGGTTGGGTGGATACC); JMJD3 (F-GGAGACCTTTATCGCCTCTG, R-TCCCTTTCACCTTGGCATT); UTX (F-GGACATGCTGTGTCACATCCT, R-CTCCTGTTGGTCTCATTTGGTG); STAT3 (F-CAGCAGCTTGACACACGGTA, R-AAACACCAAAGTGGCATGTGA), IL12RB2 (F-

ATCATGGTGGGCATTTTCTCA, R-GCTACACCACTGAGGTCTGAG); JAK2 promoter (F-GCTCTCCCCCAGCCTCTAT; R-TAGCTTCGAACTCAGCCTCC); STAT3 promoter (F-CTGGCTGAACCAAGTCATAACAC, R-TGGCTGGCTGTGCTGATAAAGC).

siRNA transfection

Naive CD4+ T cells were resuspended in 100 μl of Nucleofector solution (82 ul P3 Primary cell solution plus 18ul supplement 1, Lonza) and electroporated with 2 μM human KDM6B, human KDM6A, or human JAK2 On-TARGET plus SMART pool siRNA (Dharmacon) using the Primer T cell unstimulated HE program (Lonza). The scramble siRNA (2 uM, Invitrogen) was used for normalization. Then cells were resuspended in pre-warmed RPMI1640 medium with 10% Fetal Calf Serum (FCS) and 1% penicillin streptomycin. After 24 hours, cells were stimulated with anti- CD3/CD28 beads and harvested for further analysis at indicated time points after activation.

Flow cytometry for STAT phosphorylation, STAT3, and IL12RB2

Cells from each condition studied were harvested and washed in 2 mL of PBS without calcium and magnesium and stained for 15 minutes at room temperature with 1 uL of Zombie Violet Viability Stain (BioLegend) in 100 uL of PBS. Cells were then washed with 2 mL of FACS wash buffer (PBS with 1% fetal calf serum and 0.1% sodium azide) prior to each antibody staining protocol.

For IL12RB2, 1×10^5 cells were surface stained on ice for 15 minutes in 100 uL of FACS wash buffer with 10 uL of anti-IL-12R β2 (Miltenyi Biotec, REA333). Cells were then washed in 2 mL of FACS wash buffer and then stored in FACS fix (1X PBS with 4% paraformaldehyde) at 4°C protected from light until collection.

For STAT3, 1×10^6 cells were fixed with 1 mL of FoxP3 Fixation/Permeabilization working solution (eBioscience) for 1 hour at 4°C and washed with 2 mL of 1X Permabilization Buffer (eBioscience) and then incubated at room temperature for 1 hour in 100 uL of 1X Permeabilization buffer with 20 uL of anti-STAT3 (BD Biosciences, M59-50) protected from light. Cells were then washed in 2 mL of FACS wash buffer and stored in FACS fix at 4°C protected from light.

For phospho-flow, 1×10^6 cells were incubated at room temperature following viability staining for 1 hour at room temperature in 100 uL of 1X Permabilization buffer protected from light. Cells were then resuspended in 1 mL of cold 100% methanol and stored at −20°C until staining. Methanol fixed cells were washed with 2 mL of FACS wash buffer and stained with 5 uL of anti-pSTAT antibodies (pSTAT3, LUVNKLA, and pSTAT4, 4LURPIE, eBioscience) in 100 uL of FACS wash buffer at room temperature for 1 hour protected from light. Cells were then washed with 2 mL of FACS wash buffer and resuspended in FACS fix at 4°C protected from light until collection.

Data acquisition was conducted on an LSR-II (BD Biosciences), and analysis was performed using FlowJo (Treestar). Live cells were gated based on forward by side scatter area, and doublets were excluded based on forward scatter and side scatter height and width. Cell

populations were then gated on Zombie Violet negative cells for viability and then assessed for their respective antibody stains.

Protein purification and western blotting

Cells harvested for protein (5×10^6 cells) were washed 3 times in 1 mL of PBS without calcium and magnesium, flash frozen in liquid nitrogen, and stored at −80° C until protein isolation. Cell pellets were resuspended in 100 uL of RIPA buffer (50 mL Tris-HCl, 150 mM NaCl, 0.1% SDS, 0.5% sodium deoxycholate, 1% Triton X 100) containing complete EDTA-free protease inhibitor cocktail (Sigma Aldrich) and rotated at 4°C for 1 hour. Lysed cells were centrifuged at maximum speed at 4°C for 10 minutes, and supernatants were transferred to a fresh tube and quantitated using a BCA assay (Pierce).

For western blots, 10 ug of protein was run on a 4–12% Bis Tris gel in MOPS buffer (Novex) and transferred to a low fluorescence PVDF membrane (Immobilon-FL, Millipore). Membranes were blocked with Odyssey® blocking buffer (LI-COR) with 3% goat serum at room temperature for 2 hours and then incubated with anti-JAK2 antibody 1:1000 (Abcam, cat #ab108596) in Odyssey® blocking buffer overnight at 4°C. Membranes were washed 3 times for 5 minutes with PBS containing 0.1% Tween-20 and then incubated in IRDye 680RD Goat anti-rabbit (LI-COR) 1:10,000 in Odyssey® blocking buffer with 0.001% SDS and 0.02% Tween-20 for 45 minutes protected from light. Membranes were washed again in PBS/0.1% Tween-20 and then rinsed in deionized distilled water, and then scanned with a LI-COR Odyssey® CLx imaging system (LI-COR). Blots were stripped with Restore western blot stripping buffer (Thermo Fisher) for 20 minutes at room temperature and then blocked for 1 hour at room temperature in Odyssey® blocking buffer with 3% goat serum. Blots were then incubated with anti-alpha tubulin antibody at 1:1000 (Cell Signaling, cat #3873P) in Odyssey® buffer at 4°C for 2 hours, then washed, incubated in secondary antibody 1:10,000 (IRDye 800RD Goat anti-rabbit, LI-COR), washed and scanned as previously described for anti-JAK2. Densitometry with ImageJ was used to quantitate protein band density in scanned blot images.

***In situ* Hi-C and data analysis—**Hi-C library generation in this study was based on a previously described *in situ* Hi-C protocol (36) and was optimized for naïve CD4 T cells. Briefly, naïve CD4 T cells were fixed in culture medium containing 1% formaldehyde for 5 minutes at room temperature. 7.5 M Tris-HCl (pH 7.5) was added to a final concentration of 2.5 M to quench the formaldehyde. After washing with PBS twice, cells were resuspended in cell lysis buffer (the same recipe as JMJD3 and H3K27me3 ChIP) and incubated at 4° for 30 minutes. Nuclei were pelleted and subjected to SDS permeabilization followed by TritonX-100 to quench SDS. Nuclei pellets were then subjected to HindIII digestion and re-ligation, at which point biotin-dCTP was induced into the *de novo* ligation sites. Newly re-ligated genomic DNA was purified and sheared into 200 bp fragments, and fragments containing biotin-labeled *de novo* ligation sites were purified by M280 streptavidin beads (Invitrogen) and subjected to library preparation. Hi-C libraries were sequenced on the Illumina HiSeq 2500, targeting 100 million paired reads for each library. Hi-C reads were trimmed at the *de novo* re-ligation sites (NheI sites generated from re-ligating Hind III digestion) and then mapped to the hg38 reference genome by bowtie2. Then unique mapped

reads were subject to filtering to remove self-ligation, dangling ends and random breaking. Filtered reads were normalized by ICE method (37), and Pearson's correlation coefficient at 1 Mb resolution was calculated. As biological replicates in our data set showed high reproducibility (Pearson's correlation coefficient >0.9), all three biological replicates were combined together, and then chromatin interactions at 25 kb resolution were calculated by HOMER.

Results

ChIP-seq Quality Control

In order to determine the best region to evaluate H3K27me3 enrichment, we calculated the average distance from the transcription start sites (TSS) to H3K27me3 peaks. Others and we have recently shown that H3K4 methylation peaks are generally within 1 kb of the TSS (6, 38). In contrast, our analysis showed that H3K27me3 peaks are primarily clustered within a 2.5 kb radius of the TSS (Supplementary Figure S1A-B). Across all time points, naïve cells contained H3K27me3 peaks near a total of 5,123 gene promoters, while memory cells contained called peaks near a total of 5,490 gene promoters within this radius. Therefore, we examined H3K27me3 enrichment 2.5 kb up- and downstream of the TSS for our analyses. An ANOVA was performed to evaluate donor variability in H3K27me3 enrichment versus variability between conditions. H3K27me3 varies significantly based upon activation, time, and cell type rather than by individual donor (see p-value plots, Supplementary Figure S1C).

To determine if there was significant variation in signal-to-background ratios across samples, we plotted the distribution of coverage depths across the genome for each sample (Supplementary Figure S1D), the majority of which have consistent signal-to-background ratios. Principal coordinate analysis (39) revealed that the biological effects of interest were visible in the first 4 principal coordinates, demonstrating that technical confounding factors were not an issue (Supplementary Figure S1E–F).

In order to ensure that called peaks were robust in the face of technical and biological variation, we used the IDR framework developed for the ENCODE project. While ENCODE typically uses 2 biological replicates to assess biological reproducibility, we have 4 replicates for each group except for memory at two weeks, which only includes 3 donors. This results in 6 pairwise comparisons for each group except memory at 2 weeks with 3. For each of the pairs, the IDR method produces a count of peaks that can be confidently called at our chosen threshold of reproducibility, IDR=2%. For each group, we selected the maximum out of these 6 counts, as recommended by the ENCODE documentation for datasets of more than 2 samples. Then we selected that number of peaks from the top of the list of peaks called on the combined dataset of all replicates. The number of peaks selected for each group is shown in Supplementary Figure S1G. Since the combined peak calls are based on 4 times the sequencing depth, the peaks are called more confidently than in the individual replicates, so the 2% threshold represents an upper bound on the fraction of irreproducible peaks. The IDR thresholds were generally consistent across all replicates, and variations in number of peaks called by IDR do not associate with low signal-to-background ratios in the coverage depth distributions. Thus, the IDR threshold of 2% is well above the technical noise floor imposed by any issues with ChIP efficiency.

It is also possible that differences in ChIP efficiency could confound estimates of fold changes between sample groups. In order to assess this possible technical limitation, we looked at the MA plots of each sample versus all the other samples of the same type after normalization (Supplementary Figure S1H–I). Each MA plot generally has a low-abundance "noise mode" ($\log_2(CPM) < 2$), representing the promoters with only background noise, and a high-abundance "signal mode" ($\log_2(CPM) \approx 4.5$) representing the promoters containing ChIP signal. In the analyzed samples, the signal mode is centered vertically within 0.5 $\log_2$ fold difference of zero, indicating that the edgeR normalization used is effectively controlling for global differences in ChIP efficiency and other technical artifacts. The few samples for which the signal mode is far away from zero are samples with lower sequencing depth, which means that these samples receive less weight in the model fitting stage. Given these observations, variations in ChIP efficiency are not responsible for any perturbation larger than approximately 0.5 in reported $\log_2$ fold changes.

H3K27me3 undergoes dynamic early changes during CD4 T cell activation

To examine the dynamics of histone modifications over time, naïve (CD45RA+CD45RO−) and memory (CD45RA−CD45RO+) CD4 T cells were isolated from the peripheral blood of four healthy human donors and activated with anti-CD3/anti-CD28 beads and cultured in rIL2-supplemented media for 1 day, 5 days, and 2 weeks. Purity of each subset was >94% for all donors (Supplementary Figure S2A). ChIP-seq for H3K27me3 was performed on cells from all conditions and time points alongside RNA-seq for the same conditions. The raw data for both ChIP-seq and RNA-seq from each condition are available at the NIH Gene Expression Omnibus site (**accession #GSE73214**).

Based on our previous data, histone modifications are dynamic during CD4 T cell activation in both naïve and memory CD4 T cells (25), and this is the first kinetic study of post-activation H3K27me3 marks comparing naïve vs. memory CD4 T cells. We previously showed enrichment for H3K4me2 and H3K4me3 changes in both directions but only relatively late (i.e. 5 days post activation) in naïve and memory cells. In contrast, promoter H3K27me3 methylation changes are extensive by 1 day in both subsets (3801 genes in naïve and 1351 in memory) (Figure 1A–B). Of those gene promoters with differential H3K27me3 enrichment, 67% (2981/4473) were demethylated in naïve cells, while 98% (1548/1575) were demethylated in memory (Supplementary Figure S2B).

H3K27me3 marks differentiation-related pathways for repression throughout activation

H3K27me3 is typically considered a 'repressive' mark associated with lower gene expression. We examined the presence of H3K27me3 peaks at each time point in relation to RNA expression and verified that low expression correlated with the presence of H3K27me3 promoter peaks during activation of naïve and memory CD4 T cells (Figure 1C, 1D). We validated these results by an orthologous analysis for low versus high gene expression to compare the percentage of peaks at all time points in each subset (Figure 1E, 1F). Surprisingly, promoter H3K27me3 enrichment changes after activation of naïve cells appeared only transient, while changes in promoter H3K27me3 peak status after activation tended to correspond to more permanent chromatin remodeling, particularly for promoters gaining H3K27me3. (Supplementary Figure S2C). Interestingly, naïve cells showed a

dramatic increase in the percentage of promoters containing H3K27me3 peaks 1 day after activation (9% at rest to 23%) and ultimately maintained these marks out to 2 weeks, particularly in low expression genes. In contrast, memory cells showed very different dynamics with an increase in H3K27me3 promoter peaks at 5 days (not at 1 day). This change in state was only transient, however, and was lost by the 2 week time point (Figure 1F). The genes associated with these promoter peaks in memory mapped to embryonic stem cell pluripotency pathways, which heavily overlap with WNT signaling (Supplementary Figure S2D), and half (20 genes out of 39) overlapped with peaks gained in naïve cells at 1 day.

Gene expression for promoters gaining H3K27me3 peaks 1 day after activation of naïve cells decreased from 0 h to 2 weeks (Figure 2A) and mapped strongly to WNT signaling (Table I). We next compared the H3K27me3 peaks found in freshly isolated (“at rest”) naïve cells to those in freshly isolated resting memory cells. We discovered that memory cells had considerably more H3K27me3 promoter peaks than naïve (1891 in memory vs. 1065 in naïve with 672 shared; Figure 2B). These results suggest that pre-determined H3K27-mediated suppression of specific genes and pathways is one feature of memory cell differentiation and identity. Pathway mapping demonstrated once again that genes marked uniquely in memory cells mapped to both pluripotency and WNT signaling (Supplementary Figure S2E). We mapped the subset of genes whose H3K27me3 marks increased 1 day after naïve cell activation, which also mapped heavily to the pluripotency/WNT pathways (Table II), including WNT4 (Figure 2C) and WNT5B (Figure 2D). Additionally, this mapping identified bone morphogenic protein (BMP) and PDGF pathways, both of which have been linked to pluripotency and self-renewal (40, 41). These data strongly suggest that pathways reinforcing pluripotentiality (42) require suppression during T cell activation and differentiation.

We analyzed RNA expression to compare genes with H3K4me3 peaks from our previous data set (25) versus H3K27me3 and confirmed that genes from all conditions containing H3K27me3 promoter peaks had significantly lower RNA expression (Supplementary Figure S2F and Supplementary Table S1). Therefore, as previously described (6), genes with H3K27me3 peaks are associated with suppression of RNA expression, and this association is maintained throughout T cell activation in naïve and memory CD4 subsets.

Activation-induced changes to H3K27me3 enrichment are predicted by resting RNA expression

Why are H3K27me3 changes a primary epigenetic event in the first day after activation? Resting RNA expression is high in genes that subsequently lose H3K27me3 early after activation in both naïve and memory cells (Figure 3A–B; Supplementary Figure S2G–H). The metric used was the percentage of genes showing an increase or decrease in promoter H3K27me3 during activation compared to their RNA expression at rest. Conversely, genes with low RNA expression at rest gain H3K27me3 with activation (Figure 3A and C), but increased H3K27me3 enrichment occurs primarily in naïve and not memory cells shortly after activation (Supplementary Figure S2B). Assuming that promoter H3K27me3 exerts the canonical repressive effects described in the literature, we hypothesize that activation-

induced changes to promoter H3K27me3 enrichment early in activation function to maintain gene expression established at rest for selected genes as a function of cell type and differentiation states.

These results raise the question of how changes in H3K27me3 enrichment regulate RNA expression changes with activation. Either decreasing H3K27me3 is operating actively to increase RNA expression after activation, or this mark is passively maintaining the higher levels of expression originally determined for a selected set of genes in the resting or quiescent state. The results demonstrate that in both naïve (Figure 3D) and memory CD4 cells (Figure 3E), decreasing H3K27me3 marks in the first day correlate with higher levels of gene expression at all time points. In memory cells, there is a transient but significant increase in gene expression between rest and 1 day for promoters decreasing in H3K27me3. However, in naïve cells, overall levels of gene expression do not increase in the first 5 days after activation as would be predicted if the impact of decreased H3K27me3 was actively increasing RNA expression rather than simply reinforcing it passively.

Presumably a naïve T cell awaiting activation would have this reinforcement mechanism in place for selected genes that are critical to the process of activation. Indeed, we were able to map decreases in H3K27me3 at 1 day to numerous important canonical functions (Table III), including T cell receptor signaling (Figure 4A), apoptosis signaling, and CTLA4 signaling, all networks integrally related to T cell activation. While peaks were not always apparent in these data, a measurable decrease in enrichment occurred in many of these sites, as exemplified by the CD45 promoter in Figure 4B. In Figure 4C, we show a heat map based on hierarchical clustering of 30 selected immune activation genes in which H3K27me3 enrichment changed in either direction after activation as a function of time (resting, 1, 5 and 14 days). One gene that dramatically loses the H3K27me3 mark during activation and differentiation is DUSP4, which plays a key role in T cell proliferation (43). This gene is heavily enriched for H3K27me3 at rest in naïve and memory cells, progressing to low H3K27me3 enrichment after activation (Figure 4C–D) for both cell types with concurrent and dramatic upregulation of RNA expression by 1 day in naïve cells (Figure 4E).

H3K27me3 demethylation regulates STAT phosphorylation and T cell activation

JAK/STAT pathways were among the top canonical pathways affected by H3K27 demethylation during the early activation of naïve CD4 T cells (Figure 5A). JAK2 and STAT3 are two prominent pathway members, and their promoters are significantly demethylated 1 day after activation (Figure 5B–C). JAK2 phosphorylates several STATs in multiple pathways, including the IL12 receptor pathway mediated by STAT3 and STAT4, which is necessary for Th1 differentiation (44). Treatment of naïve CD4 T cells with the selective H3K27 demethylase inhibitor, GSK-J4 (45), increased H3K27me3 at the *JAK2* and *STAT3* promoters with a concomitant decrease in RNA expression of *JAK2* and *STAT3* (Figure 5D). Since GSK-J4 inhibits both known H3K27 demethylases, JMJD3 and UTX (45), knockdowns of each were performed. In JMJD3 knockdowns, *JAK2* expression was decreased 8 hours after activation, while *JAK2* expression in UTX knockdowns was not significantly different than scrambled controls. In contrast, *STAT3* expression was significantly decreased 8 hours after activation in both JMJD3 and UTX knockdowns

(Figure 5E, Supplementary Figure S2I–J). Protein expression of both JAK2 and STAT3 was reduced in GSK-J4 treated cells compared to vehicle controls (Figure 5F–G).

Phosphorylation of both JAK2 targets, STAT3 and STAT4, was impaired in GSK-J4 treated cells (Figure 6A). Knockdown of JAK2 confirmed that impaired phosphorylation of STAT3 and STAT4 results from the loss of JAK2 expression (Figure 6B, Supplementary Figure S2K). Interestingly, addition of IL-6, a known proinflammatory cytokine whose receptor signals through JAK1 (46), resulted in a rescue of STAT3 phosphorylation in GSK-J4 treated cells (Figure 6C). RNA-seq of JMJD3 knockdowns 1 day after activation revealed that IL12RB2 and JMJD3 (KDM6B) were the top 3 and 4 most differentially expressed and down-regulated genes (FDR <10%) compared to scramble siRNA controls (Figure 6D, Supplementary Table S2). Additionally, GSK-J4 treated cells showed a decrease in IL12RB2 surface expression (Figure 6E). Since pSTAT4 drives transcription of IL12RB2, we hypothesized that decreased JAK2 expression was responsible for this effect. Indeed, JAK2 knockdown in naïve CD4 T cells showed a comparable decrease in IL12RB2 mRNA to JMJD3 knockdowns (Figure 6F, Supplementary Figure S2L). We then did ChIP-seq for JMJD3 and UTX. Analysis of the IL12RB2 gene revealed peaks of JMJD3 but not UTX binding at 8 hours post activation (Figure 6G). Of three JMJD3 binding sites, all located in the introns of IL12RB2, two sites matched perfectly to the loss of H3K27me3 peaks at 24 hours.

While no JMJD3 or UTX peaks were found in the *JAK2* promoter, two JMJD3 peaks surrounding the *JAK2* locus were identified (Figure 7A). One peak (Chr. 9–7) was located 10 kb upstream of the *JAK2* TSS and was associated with a reduction in H3K27me3 at that site after activation (Figure 7B and 7D), while the other (Chr. 9–10) was located 1.66 mb downstream of the *JAK2* TSS and did not exhibit a reduction in H3K27me3 (Figure 7C and 7E). The two JMJD3 peaks overlapped with H3K4me1 peaks and DNase Hypersensitivity Sites (DHS) found in ENCODE for human CD4+ T cells. Additionally, no H3K27ac peaks were observed at these sites, consistent with previously described silencing enhancer sites (47, 48). HiC revealed that the distal peak interacts with the *JAK2* promoter (Figure 7A), suggesting a mechanism for the significantly decreased H3K27me3 surrounding the TSS and further supporting JMJD3's involvement in the regulation of this gene. No JMJD3 or UTX peaks were identified surrounding the *STAT3* locus, and HiC did not reveal any distal JMJD3 sites interacting with the promoter, calling into question how the observed loss of H3K27me3 around the *STAT3* promoter is occurring.

Taken together, these data suggest that H3K27 demethylation during naïve T cell activation is critical for regulating at least two well-established pathways important for T cell function and differentiation (44, 49). However, 34 other significantly differentially expressed genes were seen in the JMJD3 knockdowns (Supplementary Table S2), the majority of which are also established in T cell activation and differentiation pathways as worthy candidates for future studies to build on our current work.

Discussion

Based on our results, loss of H3K27me3 during CD4 T cell activation participates in the regulation of several genes key to CD4 T cell function, including JAK2, STAT3, and IL12RB2. Conversely, the addition of H3K27me3 during naïve CD4 T cell activation targets pluripotency related genes, and these marks are perpetuated in memory cells. Our results demonstrate that promoter H3K27me3 fits the paradigm of a 'repressive' mark in CD4 T cells, associating with low expression genes throughout activation in both naïve and memory CD4 T cells. The mechanisms behind H3K27me3-mediated silencing are not well characterized, and little is known about how these mechanisms are regulated during immune activation of CD4 naïve vs. memory cells. Polycomb repressive complex 2 (PRC2) is responsible for H3K27 methylation, and conventional thinking is that silencing mediated by H3K27me3 is due to binding of the modified histone by the Polycomb Repressive Complex 1 (PRC1) (50, 51). H3K27me3 has been proposed to be a marker deposited in association with gene silencing and not a direct cause of it (51, 52). In fact, contrary to the paradigm that H3K27me3 is a repressive mark, promoter H3K27me3 in ES cells has been shown to associate with actively transcribed promoters (32). In contrast, our data, as well as previous data from CD4 T cells (6), suggest a strong correlation between the presence of promoter H3K27me3 and gene silencing, with the vast majority of genes containing H3K27me3 in their promoters demonstrating a low level of expression.

Loss of H3K27me3 enrichment was a prominent finding early after T cell activation (i.e. day 1) in both subsets. However, naïve CD4 T cells demonstrated a simultaneous gain of H3K27me3 enrichment in 1492 gene promoters, and that gain was also associated with low gene expression at rest. This low expression state remains consistent for these same genes at all time points studied after activation, and many maintained additional H3K27me3 peaks in resting memory cells. Thus, for this subset of genes, increasing H3K27me3 at day 1 after CD4 T cell activation appears to reinforce low gene expression. Based on current literature, we speculate that the mechanism is binding of PRC to the histones with this modification. Mapping of this subset of 1492 genes revealed connections to WNT signaling and pluripotency pathways. Importantly, in contrast to naïve CD4, relatively few genes show increased promoter enrichment of H3K27me3 in activated memory cells, suggesting one feature of naïve T cell activation is a need to maintain a subset of genes in a repressed state. On the other hand, memory cells demonstrate far more H3K27me3 promoter peaks at rest, many of which are concomitant with increased promoter enrichment and H3K27me3 peak gain in naïve cells after activation. These genes also map to the same WNT-related pluripotency pathways. Therefore, we conclude that during CD4 memory cell commitment, this subset of critical genes has already been marked for repression. WNT signaling was previously shown to maintain a pool of undifferentiated cells for further selection, differentiation, and effector function (42), suggesting that its repression during activation might promote T cell differentiation.

It is clear that many changes to promoter enrichment for H3K27me3 after activation correlate with basal RNA expression at rest for both naïve and memory cells (Figure 3A–C, Supplementary Figure S2F–G). Thus, genes showing an activation-induced increase in promoter H3K27me3 enrichment demonstrate low gene expression prior to activation, while

genes showing a decrease in promoter H3K27me3 enrichment have higher levels of gene expression at rest. Loss of overall H3K27me3 enrichment is a profound change after activation in both naïve and memory CD4 T cells and appears to be mostly transient. Our data show this loss is associated with consistently higher gene expression for affected genes at all time points studied (Figure 3D–E). Mechanistically this might occur via the recognition by H3K27 demethylases of areas featuring partially open chromatin during the resting state and subsequent removal of H3K27 methylation early in activation to open these regions completely and reinforce baseline gene expression. Not surprisingly, genes affected by this epigenetic regulatory mechanism map to pathways highly important for T cell activation, such as T cell receptor and interleukin signaling (Table III). Recent work has demonstrated that the H3K27me3 demethylase, JMJD3, is necessary for Th1 polarization during CD4 T cell differentiation, and Jmjd3 deficiency in mice resulted in a loss of plasticity in CD4 T cells, supporting our results that H3K27me3 demethylation is integral for CD4 T cell function (15). The other H3K27 demethylase, UTX, has not been evaluated in this context, but our data with UTX knockdowns do not suggest it is critical for early activation events in CD4 cells. Indeed, JMJD3 is upregulated in response to numerous stimuli, while UTX is described as more of a maintenance demethylase with ubiquitous expression (53, 54). How regulation and specific gene targeting by either enzyme is accomplished to support CD4 T cell agendas is clearly going to be important to study.

The JAK-STAT pathways are heavily represented in our pathway mapping of H3K27 demethylation (Figure 5A). Our explorations of the role of H3K27 demethylation in JAK2 and STAT3 gene expression demonstrate that this mechanism is important for maintaining their high expression during activation. Thus, inhibition of H3K27 demethylation during activation results in increased promoter H3K27me3 and decreased expression of these genes (Figure 5C–G). In our studies, JMJD3 appears to be solely responsible for the demethylation of the *JAK2* promoter, while H3K27 demethylation of the *STAT3* promoter is affected by siRNA-driven loss of either JMJD3 or UTX (Figure 5D). Interestingly, previous reports demonstrated that Stat3, in addition to Stat1, are responsible for transcription of *Jmjd3* in rat microglial cells (55), suggesting there might be a feedback loop between JMJD3 and STAT3. However, in our data we were never able to prove a direct interaction of JMJD3 with the *STAT3* promoter or with any distal elements interacting with the *STAT3* promoter, rendering us unable to support this conclusion in the context of CD4 T cells. Knock-out of *Jak2* in mice is embryonic lethal from severe defects in hematopoiesis (56, 57). Conditional knock-outs also suffer defects in hematopoiesis, with the erythroid and thrombocytic stem cell compartments primarily affected (58–60). Naturally occurring and activating somatic mutations of *JAK2* in humans have also been documented to result in myeloproliferative syndromes (56–58).

The knowledge surrounding the pairing of JAKs with specific receptors has been complicated by the fact that they frequently can substitute for each other (61). Nonetheless, these same studies demonstrate that JAK2 is a necessary molecule for cellular function. Indeed, in our studies, loss of JAK2 resulted in reduced phosphorylation of STAT3 and STAT4 (Figure 6B) as well as subsequent reduction of IL12RB2 RNA expression (Figure 6F), all of which are integral for Th1 differentiation (44). Thus, loss of JMJD3 resulting in a reduction in JAK2 is likely to be at least partially responsible for the skewing away from

Th1 differentiation observed in Jmjd3 knock-out mice (15). Additionally, we used ChIP-seq to demonstrate the direct binding of JMJD3 to the *IL12RB2* gene outside of the promoter (but within the 2.5 kb radius of the TSS), which corresponds to the loss of its H3K27me3 peaks downstream of the promoter and the transcriptional start site (Figure 6G) 1 day after activation. Strikingly, our data demonstrate that the loss of these peaks is perpetuated long term, as resting memory cells do not contain them. It has previously been shown that JMJD3 is a requirement for RNA Polymerase II to progress through gene bodies enriched with H3K27me3 (62). We reason that the site-specific loss of the repression-associated H3K27me3 peak also contributes directly to the dramatic decrease in IL12RB2 gene expression seen in the JMJD3 knockdowns (Figure 6D).

H3K27me3 has been characterized as an important epigenetic mark for CD4 T cell differentiation. In contrast to the Th2 polarization that occurs in the absence of JMJD3, CD4 T cells lacking EZH2, the central component of PRC2, will overproduce IFN-γ and skew toward a Th1 phenotype (63). Our data did not demonstrate any clear differential enrichment for H3K27me3 at the IFN-γ promoter or its interacting distal elements; however, we cultured our cells under non-polarizing conditions that result in a mixture of Th subtypes after activation. Therefore, Th subset-specific peaks will not necessarily be prominent in our data. Considering the heavy impact of H3K27me3-mediated mechanisms upon the expression of *IL12RB2*, which regulates IFN-γ production upstream, we propose that the effects upon IFN-γ are indirect in human CD4 T cells and a direct result of both defective JAK2 signaling and decreased *IL12RB2* expression. Indeed, we were able to show clearly that loss of JAK2 in GSK-J4 treated cells (a small molecule inhibitor of JMJD3 and UTX) resulted in reduced phosphorylation of both STAT3 and STAT4. Additionally, this was not an off-target effect of the drug, as STAT3 phosphorylation could be rescued by the addition of IL-6 (whose receptor signals through JAK1), and knockdowns of JMJD3 demonstrated the same effect.

One limitation of the current study is that we restricted most of our analysis to regions within 2.5 kb of the TSS. As described in our results, this distance was calculated based upon the average distance of H3K27me3 peak summits from the TSS, the majority of which fell within a 2.5 kb radius (Supplementary Figure 1A). This result suggested that H3K27me3 peaks generally fell within 2.5 kb of the TSS. As previously reported, H3K27me3 peaks primarily affect gene promoters containing CpG islands (CGI) (64). In our data, we found that approximately 85% of the gene promoters with called H3K27me3 peaks near the TSS contained CGI, which supports that conclusion that the skewing of H3K27me3 peaks toward the TSS is being driven by CGI promoters. Additionally, it became clear during our mechanistic studies evaluating the role of JMJD3 in *JAK2* expression that the loss of H3K27me3 in regions outside the specified radius was potentially an important mechanism, despite the fact that the majority of H3K27me3 peaks were not called in these genomic territories. Therefore, we are currently performing further analyses to assess the role of JMJD3 and H3K27me3 loss in these regions.

Another limitation of the current study is the potential for some of the effects observed on gene expression to be perpetuated from altered expression of upstream regulators. Technology does not currently allow manipulation of H3K27 demethylase activity targeted

to specific loci, which makes the study of direct H3K27me3 effects challenging. Because of the broad activity encompassed by GSK-J4 as well as siRNAs targeting JMJD3 and UTX, we attempted to examine the H3K27me3 status of the pathway members we evaluated in detail in order to compensate for this difficulty. However, we acknowledge that upstream regulators that are currently not mapped to the JAK-STAT and IL12RB2 pathways could also be playing a role in the altered expression of some of these genes.

Ultimately, this study demonstrates that the states of H3K27me3 in promoters are highly dynamic during CD4 T cell activation, and that these dynamics differ markedly between naïve and memory cells. Both T cell subsets rely upon H3K27me3 demethylation by JMJD3 during activation to facilitate and maintain high expression of genes that are crucial to T cell function and differentiation. Conversely, naïve cells are unique in increasing H3K27me3 enrichment in genes pertinent to differentiation-related pathways, and these immune activation-induced marks are maintained in cells that enter the memory effector pool. Further studies will explore How H3K27me3 dynamics in other genomic regions affect CD4 T cell function to broaden our understanding of this important epigenetic mark.

Supplementary Material

Refer to Web version on PubMed Central for supplementary material.

Acknowledgments

We thank Dwight Kono, Michael McHeyzer-Williams, and Peiqing Sun for their input into this work.

This research was supported by funds from the National Institutes of Health: U19 AI063603 (DRS), 1TL1 TR001113-01 (SAL), T32 DK007022-30, Postdoctoral Juvenile Diabetes Research Foundation fellowship (HKK), Predoctoral Mendez National Transplantation Institute's Fund (XM) and the Verna Harrah Research Funds supporting the Salomon laboratory.

References

1. Rothbart SB, Strahl BD. Interpreting the language of histone and DNA modifications. Biochimica et biophysica acta. 2014; 1839:627–643. [PubMed: 24631868]
2. Lessard JA, Crabtree GR. Chromatin regulatory mechanisms in pluripotency. Annual review of cell and developmental biology. 2010; 26:503–532.
3. Tee WW, Reinberg D. Chromatin features and the epigenetic regulation of pluripotency states in ESCs. Development. 2014; 141:2376–2390. [PubMed: 24917497]
4. Vastenhouw NL, Schier AF. Bivalent histone modifications in early embryogenesis. Current opinion in cell biology. 2012; 24:374–386. [PubMed: 22513113]
5. Neff T, Armstrong SA. Chromatin maps, histone modifications and leukemia. Leukemia. 2009; 23:1243–1251. [PubMed: 19322211]
6. Barski A, Cuddapah S, Cui K, Roh TY, Schones DE, Wang Z, Wei G, Chepelev I, Zhao K. High-resolution profiling of histone methylations in the human genome. Cell. 2007; 129:823–837. [PubMed: 17512414]
7. Wei G, Wei L, Zhu J, Zang C, Hu-Li J, Yao Z, Cui K, Kanno Y, Roh TY, Watford WT, Schones DE, Peng W, Sun HW, Paul WE, O'Shea JJ, Zhao K. Global mapping of H3K4me3 and H3K27me3 reveals specificity and plasticity in lineage fate determination of differentiating CD4+ T cells. Immunity. 2009; 30:155–167. [PubMed: 19144320]
8. Russ BE, Olshanksy M, Smallwood HS, Li J, Denton AE, Prier JE, Stock AT, Croom HA, Cullen JG, Nguyen ML, Rowe S, Olson MR, Finkelstein DB, Kelso A, Thomas PG, Speed TP, Rao S,

Turner SJ. Distinct epigenetic signatures delineate transcriptional programs during virus-specific CD8(+) T cell differentiation. Immunity. 2014; 41:853–865. [PubMed: 25517617]

9. Wang Z, Zang C, Rosenfeld JA, Schones DE, Barski A, Cuddapah S, Cui K, Roh TY, Peng W, Zhang MQ, Zhao K. Combinatorial patterns of histone acetylations and methylations in the human genome. Nature genetics. 2008; 40:897–903. [PubMed: 18552846]
10. Zhang JA, Mortazavi A, Williams BA, Wold BJ, Rothenberg EV. Dynamic transformations of genome-wide epigenetic marking and transcriptional control establish T cell identity. Cell. 2012; 149:467–482. [PubMed: 22500808]
11. Lim PS, Hardy K, Bunting KL, Ma L, Peng K, Chen X, Shannon MF. Defining the chromatin signature of inducible genes in T cells. Genome biology. 2009; 10:R107. [PubMed: 19807913]
12. Barski A, Jothi R, Cuddapah S, Cui K, Roh TY, Schones DE, Zhao K. Chromatin poises miRNA- and protein-coding genes for expression. Genome research. 2009; 19:1742–1751. [PubMed: 19713549]
13. Allan RS, Zueva E, Cammas F, Schreiber HA, Masson V, Belz GT, Roche D, Maison C, Quivy JP, Almouzni G, Amigorena S. An epigenetic silencing pathway controlling T helper 2 cell lineage commitment. Nature. 2012; 487:249–253. [PubMed: 22763435]
14. Zhou VW, Goren A, Bernstein BE. Charting histone modifications and the functional organization of mammalian genomes. Nature reviews Genetics. 2011; 12:7–18.
15. Li Q, Zou J, Wang M, Ding X, Chepelev I, Zhou X, Zhao W, Wei G, Cui J, Zhao K, Wang HY, Wang RF. Critical role of histone demethylase Jmjd3 in the regulation of CD4+ T-cell differentiation. Nature communications. 2014; 5:5780.
16. Vahedi G, Kanno Y, Sartorelli V, O'Shea JJ. Transcription factors and CD4 T cells seeking identity: masters, minions, setters and spikers. Immunology. 2013; 139:294–298. [PubMed: 23586907]
17. Manna S, Kim JK, Bauge C, Cam M, Zhao Y, Shetty J, Vacchio MS, Castro E, Tran B, Tessarollo L, Bosselut R. Histone H3 Lysine 27 demethylases Jmjd3 and Utx are required for T-cell differentiation. Nature communications. 2015; 6:8152.
18. Agger K, Cloos PA, Christensen J, Pasini D, Rose S, Rappsilber J, Issaeva I, Canaani E, Salcini AE, Helin K. UTX and JMJD3 are histone H3K27 demethylases involved in HOX gene regulation and development. Nature. 2007; 449:731–734. [PubMed: 17713478]
19. Morales Torres C, Laugesen A, Helin K. Utx is required for proper induction of ectoderm and mesoderm during differentiation of embryonic stem cells. PloS one. 2013; 8:e60020. [PubMed: 23573229]
20. De Santa F, Narang V, Yap ZH, Tusi BK, Burgold T, Austenaa L, Bucci G, Caganova M, Notarbartolo S, Casola S, Testa G, Sung WK, Wei CL, Natoli G. Jmjd3 contributes to the control of gene expression in LPS-activated macrophages. The EMBO journal. 2009; 28:3341–3352. [PubMed: 19779457]
21. Barradas M, Anderton E, Acosta JC, Li S, Banito A, Rodriguez-Niedenfuhr M, Maertens G, Banck M, Zhou MM, Walsh MJ, Peters G, Gil J. Histone demethylase JMJD3 contributes to epigenetic control of INK4a/ARF by oncogenic RAS. Genes Dev. 2009; 23:1177–1182. [PubMed: 19451218]
22. Mansour AA, Gafni O, Weinberger L, Zviran A, Ayyash M, Rais Y, Krupalnik V, Zerbib M, Amann-Zalcenstein D, Maza I, Geula S, Viukov S, Holtzman L, Pribluda A, Canaani E, Horn-Saban S, Amit I, Novershtern N, Hanna JH. The H3K27 demethylase Utx regulates somatic and germ cell epigenetic reprogramming. Nature. 2012; 488:409–413. [PubMed: 22801502]
23. Zhao W, Li Q, Ayers S, Gu Y, Shi Z, Zhu Q, Chen Y, Wang HY, Wang RF. Jmjd3 inhibits reprogramming by upregulating expression of INK4a/Arf and targeting PHF20 for ubiquitination. Cell. 2013; 152:1037–1050. [PubMed: 23452852]
24. Ntziachristos P, Tsirigos A, Welstead GG, Trimarchi T, Bakogianni S, Xu L, Loizou E, Holmfeldt L, Strikoudis A, King B, Mullenders J, Becksfort J, Nedjic J, Paietta E, Tallman MS, Rowe JM, Tonon G, Satoh T, Kruidenier L, Prinjha R, Akira S, Van Vlierberghe P, Ferrando AA, Jaenisch R, Mullighan CG, Aifantis I. Contrasting roles of histone 3 lysine 27 demethylases in acute lymphoblastic leukaemia. Nature. 2014; 514:513–517. [PubMed: 25132549]
25. LaMere SA, Thompson RC, Komori HK, Mark A, Salomon DR. Promoter H3K4 methylation dynamically reinforces activation-induced pathways in human CD4 T cells. Genes Immun. 2016

26. Head SR, Komori HK, Hart GT, Shimashita J, Schaffer L, Salomon DR, Ordoukhanian PT. Method for improved Illumina sequencing library preparation using NuGEN Ovation RNA-Seq System. BioTechniques. 2011; 50:177–180. [PubMed: 21486238]
27. Langmead B, Salzberg SL. Fast gapped-read alignment with Bowtie 2. Nat Methods. 2012; 9:357–359. [PubMed: 22388286]
28. Lun AT, Smyth GK. De novo detection of differentially bound regions for ChIP-seq data using peaks and windows: controlling error rates correctly. Nucleic acids research. 2014; 42:e95. [PubMed: 24852250]
29. Lund SP, Nettleton D, McCarthy DJ, Smyth GK. Detecting differential expression in RNA-sequence data using quasi-likelihood with shrunken dispersion estimates. Statistical applications in genetics and molecular biology. 2012:11.
30. Benjamini YH, Yosef. Controlling the false discovery rate: a practical and powerful approach to multiple testing. Journal of the Royal Statistical Society Series B (Methodological). 1995; 57:289–300.
31. Pekowska A, Benoukraf T, Ferrier P, Spicuglia S. A unique H3K4me2 profile marks tissue-specific gene regulation. Genome research. 2010; 20:1493–1502. [PubMed: 20841431]
32. Young MD, Willson TA, Wakefield MJ, Trounson E, Hilton DJ, Blewitt ME, Oshlack A, Majewski IJ. ChIP-seq analysis reveals distinct H3K27me3 profiles that correlate with transcriptional activity. Nucleic acids research. 2011; 39:7415–7427. [PubMed: 21652639]
33. Chakraborty AK, Weiss A. Insights into the initiation of TCR signaling. Nature immunology. 2014; 15:798–807. [PubMed: 25137454]
34. Kim D, Pertea G, Trapnell C, Pimentel H, Kelley R, Salzberg SL. TopHat2: accurate alignment of transcriptomes in the presence of insertions, deletions and gene fusions. Genome biology. 2013; 14:R36. [PubMed: 23618408]
35. Livak KJ, Schmittgen TD. Analysis of relative gene expression data using real-time quantitative PCR and the 2(-Delta Delta C(T)) Method. Methods. 2001; 25:402–408. [PubMed: 11846609]
36. Rao SSP, Huntley MH, Durand NC, Stamenova EK, Bochkov ID, Robinson JT, Sanborn AL, Machol I, Omer AD, Lander ES, Aiden EL. A 3D Map of the Human Genome at Kilobase Resolution Reveals Principles of Chromatin Looping. Cell. 2014; 159:1665–1680. [PubMed: 25497547]
37. Imakaev M, Fudenberg G, McCord RP, Naumova N, Goloborodko A, Lajoie BR, Dekker J, Mirny LA. Iterative correction of Hi-C data reveals hallmarks of chromosome organization. Nature methods. 2012; 9:999–1003. [PubMed: 22941365]
38. Komori HK, Hart T, LaMere SA, Chew PV, Salomon DR. Defining CD4 T cell memory by the epigenetic landscape of CpG DNA methylation. Journal of immunology. 2015; 194:1565–1579.
39. Gower JC. Some Distance Properties of Latent Root and Vector Methods Used in Multivariate Analysis. Biometrika. 1966; 53:325–338.
40. Kondo T, Raff M. Oligodendrocyte precursor cells reprogrammed to become multipotential CNS stem cells. Science. 2000; 289:1754–1757. [PubMed: 10976069]
41. Fiedler J, Roderer G, Gunther KP, Brenner RE. BMP-2, BMP-4, and PDGF-bb stimulate chemotactic migration of primary human mesenchymal progenitor cells. Journal of cellular biochemistry. 2002; 87:305–312. [PubMed: 12397612]
42. Staal FJ, Luis TC, Tiemessen MM. WNT signalling in the immune system: WNT is spreading its wings. Nature reviews Immunology. 2008; 8:581–593.
43. Huang CY, Lin YC, Hsiao WY, Liao FH, Huang PY, Tan TH. DUSP4 deficiency enhances CD25 expression and CD4+ T-cell proliferation without impeding T-cell development. European journal of immunology. 2012; 42:476–488. [PubMed: 22101742]
44. Jacobson NG, Szabo SJ, Guler ML, Gorham JD, Murphy KM. Regulation of interleukin-12 signal transduction during T helper phenotype development. Res Immunol. 1995; 146:446–456. [PubMed: 8839144]
45. Kruidenier L, Chung CW, Cheng Z, Liddle J, Che K, Joberty G, Bantscheff M, Bountra C, Bridges A, Diallo H, Eberhard D, Hutchinson S, Jones E, Katso R, Leveridge M, Mander PK, Mosley J, Ramirez-Molina C, Rowland P, Schofield CJ, Sheppard RJ, Smith JE, Swales C, Tanner R, Thomas P, Tumber A, Drewes G, Oppermann U, Patel DJ, Lee K, Wilson DM. A selective jumonji

H3K27 demethylase inhibitor modulates the proinflammatory macrophage response. Nature. 2012; 488:404–408. [PubMed: 22842901]

46. Heinrich PC, Behrmann I, Muller-Newen G, Schaper F, Graeve L. Interleukin-6-type cytokine signalling through the gp130/Jak/STAT pathway. The Biochemical journal. 1998; 334(Pt 2):297–314. [PubMed: 9716487]
47. Rada-Iglesias A, Bajpai R, Swigut T, Brugmann SA, Flynn RA, Wysocka J. A unique chromatin signature uncovers early developmental enhancers in humans. Nature. 2011; 470:279–283. [PubMed: 21160473]
48. Calo E, Wysocka J. Modification of enhancer chromatin: what, how, and why? Molecular cell. 2013; 49:825–837. [PubMed: 23473601]
49. Egwuagu CE. STAT3 in CD4+ T helper cell differentiation and inflammatory diseases. Cytokine. 2009; 47:149–156. [PubMed: 19648026]
50. Fischle W, Wang Y, Jacobs SA, Kim Y, Allis CD, Khorasanizadeh S. Molecular basis for the discrimination of repressive methyl-lysine marks in histone H3 by Polycomb and HP1 chromodomains. Genes Dev. 2003; 17:1870–1881. [PubMed: 12897054]
51. Simon JA, Kingston RE. Occupying chromatin: Polycomb mechanisms for getting to genomic targets, stopping transcriptional traffic, and staying put. Molecular cell. 2013; 49:808–824. [PubMed: 23473600]
52. Henikoff S, Shilatifard A. Histone modification: cause or cog? Trends in genetics : TIG. 2011; 27:389–396. [PubMed: 21764166]
53. Burgold T, Spreafico F, De Santa F, Totaro MG, Prosperini E, Natoli G, Testa G. The histone H3 lysine 27-specific demethylase Jmjd3 is required for neural commitment. PloS one. 2008; 3:e3034. [PubMed: 18716661]
54. Sen GL, Webster DE, Barragan DI, Chang HY, Khavari PA. Control of differentiation in a self-renewing mammalian tissue by the histone demethylase JMJD3. Genes Dev. 2008; 22:1865–1870. [PubMed: 18628393]
55. Przanowski P, Dabrowski M, Ellert-Miklaszewska A, Kloss M, Mieczkowski J, Kaza B, Ronowicz A, Hu F, Piotrowski A, Kettenmann H, Komorowski J, Kaminska B. The signal transducers Stat1 and Stat3 and their novel target Jmjd3 drive the expression of inflammatory genes in microglia. J Mol Med (Berl). 2014; 92:239–254. [PubMed: 24097101]
56. Neubauer H, Cumano A, Muller M, Wu H, Huffstadt U, Pfeffer K. Jak2 deficiency defines an essential developmental checkpoint in definitive hematopoiesis. Cell. 1998; 93:397–409. [PubMed: 9590174]
57. Parganas E, Wang D, Stravopodis D, Topham DJ, Marine JC, Teglund S, Vanin EF, Bodner S, Colamonici OR, van Deursen JM, Grosveld G, Ihle JN. Jak2 is essential for signaling through a variety of cytokine receptors. Cell. 1998; 93:385–395. [PubMed: 9590173]
58. Park SO, Wamsley HL, Bae K, Hu Z, Li X, Choe SW, Slayton WB, Oh SP, Wagner KU, Sayeski PP. Conditional deletion of Jak2 reveals an essential role in hematopoiesis throughout mouse ontogeny: implications for Jak2 inhibition in humans. PloS one. 2013; 8:e59675. [PubMed: 23544085]
59. Grisouard J, Hao-Shen H, Dirnhofer S, Wagner KU, Skoda RC. Selective deletion of Jak2 in adult mouse hematopoietic cells leads to lethal anemia and thrombocytopenia. Haematologica. 2014; 99:e52–54. [PubMed: 24510341]
60. Akada H, Akada S, Hutchison RE, Sakamoto K, Wagner KU, Mohi G. Critical role of Jak2 in the maintenance and function of adult hematopoietic stem cells. Stem cells. 2014; 32:1878–1889. [PubMed: 24677703]
61. Babon JJ I, Lucet S, Murphy JM, Nicola NA, Varghese LN. The molecular regulation of Janus kinase (JAK) activation. The Biochemical journal. 2014; 462:1–13. [PubMed: 25057888]
62. Estaras C, Fueyo R, Akizu N, Beltran S, Martinez-Balbas MA. RNA polymerase II progression through H3K27me3-enriched gene bodies requires JMJD3 histone demethylase. Mol Biol Cell. 2013; 24:351–360. [PubMed: 23243002]
63. Antignano F, Zaph C. Regulation of CD4 T-cell differentiation and inflammation by repressive histone methylation. Immunology and cell biology. 2015; 93:245–252. [PubMed: 25582341]

64. Mikkelsen TS, Ku M, Jaffe DB, Issac B, Lieberman E, Giannoukos G, Alvarez P, Brockman W, Kim TK, Koche RP, Lee W, Mendenhall E, O'Donovan A, Presser A, Russ C, Xie X, Meissner A, Wernig M, Jaenisch R, Nusbaum C, Lander ES, Bernstein BE. Genome-wide maps of chromatin state in pluripotent and lineage-committed cells. Nature. 2007; 448:553–560. [PubMed: 17603471]

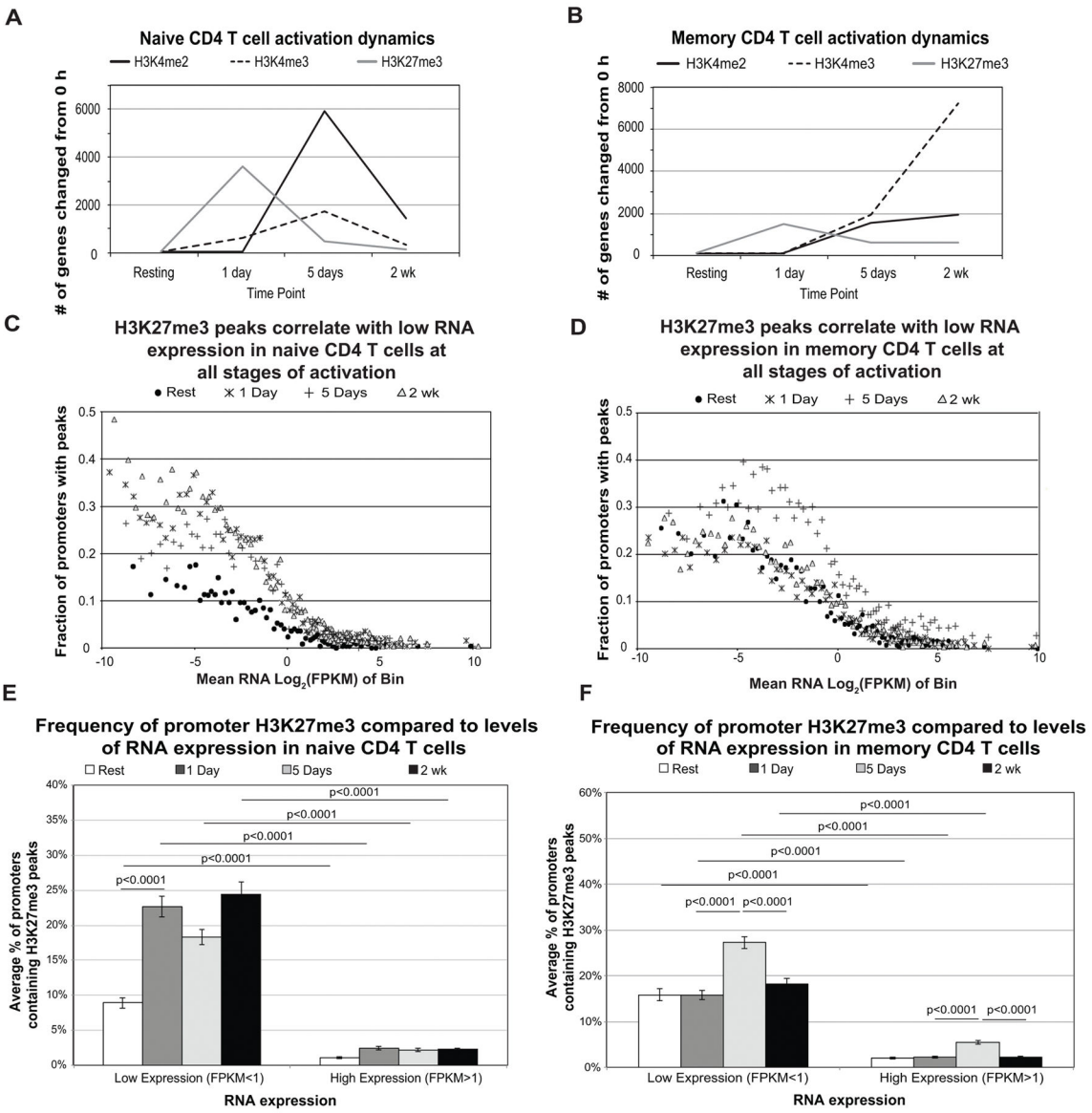

Figure 1. The presence of H3K27me3 peaks correlates with low RNA expression throughout CD4 T cell activation

H3K27me3 and H3K4me enrichment are dynamic throughout activation for both naïve **A)** and memory **B)** subsets. **C)** Promoter H3K27me3 peaks correlate with low RNA expression throughout activation of naïve CD4 T cells. Bins of 250 genes were plotted for mean RNA expression and % of promoters containing H3K27me3 peaks at all time points examined. **D)** Analysis for memory CD4 T cells as for naïve in **C). E)** Lowly expressed genes have significantly more promoters with H3K27me3 peaks in naïve cells. Genes were divided into low (FPKM<1) and high (FPKM>1) expression and plotted against their average promoter H3K27me3 peak percentage for all time points examined (resting, 1 day, 5 days, and 2 weeks) in naïve CD4 T cells. Error bars represent variance from one-way ANOVA. Reported p-values are from Tukey's HSD post-hoc analysis. **F)** Analysis for memory cells as for naïve in **C)**.

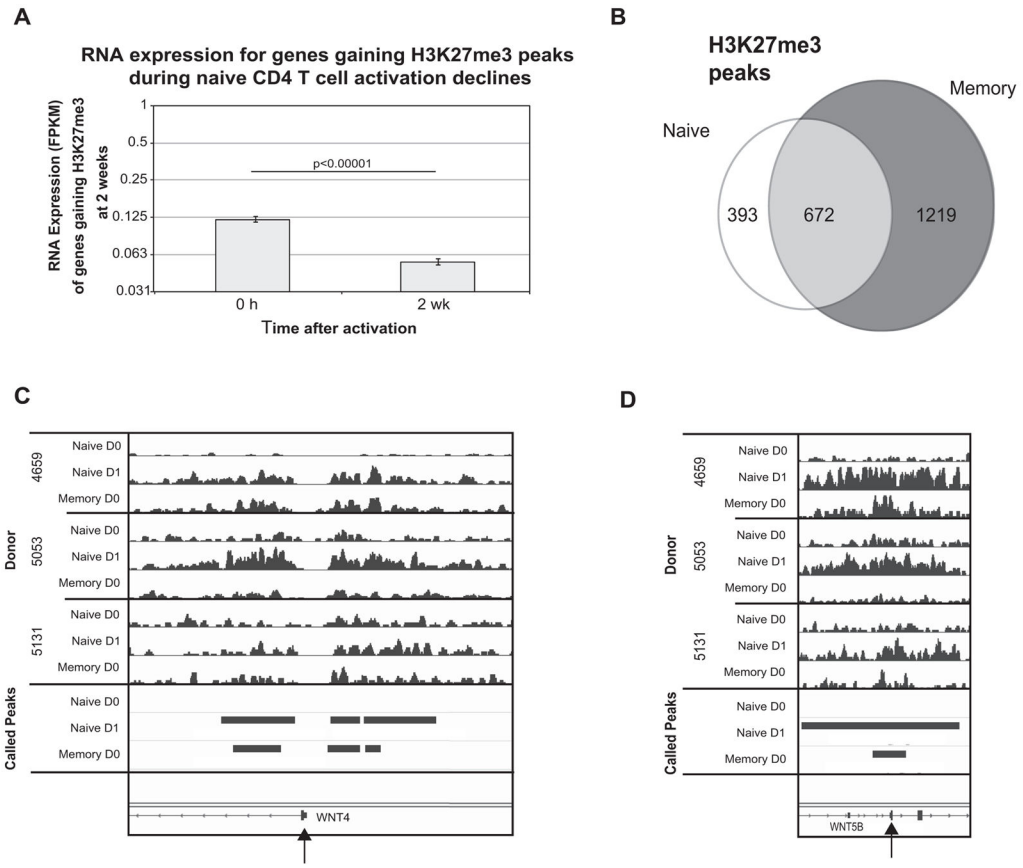

Figure 2. H3K27me3 peaks appearing after activation and during memory formation are associated with a decrease in RNA expression over time and map to WNT signaling

A) Mean RNA expression for genes that have gained H3K27me3 promoter peaks 1 day after activation of naïve CD4 T cells at rest and at 2 weeks. Error bars represent standard error of the mean. Reported p-value is from two-tailed student t-test. **B)** Venn diagram illustrating the number of called H3K27me3 promoter peaks in freshly isolated resting naïve and memory CD4 T cells. Genome viewer pile-ups of H3K27me3 from three donors shows an increase in H3K27me3 from naïve at rest vs. naïve at 1 day and memory at rest surrounding the WNT4 **(D)** and WNT5B **(D)** promoters, with called peaks appearing 1 day after activation and in resting memory cells. The region with the arrow represents the affected promoter.

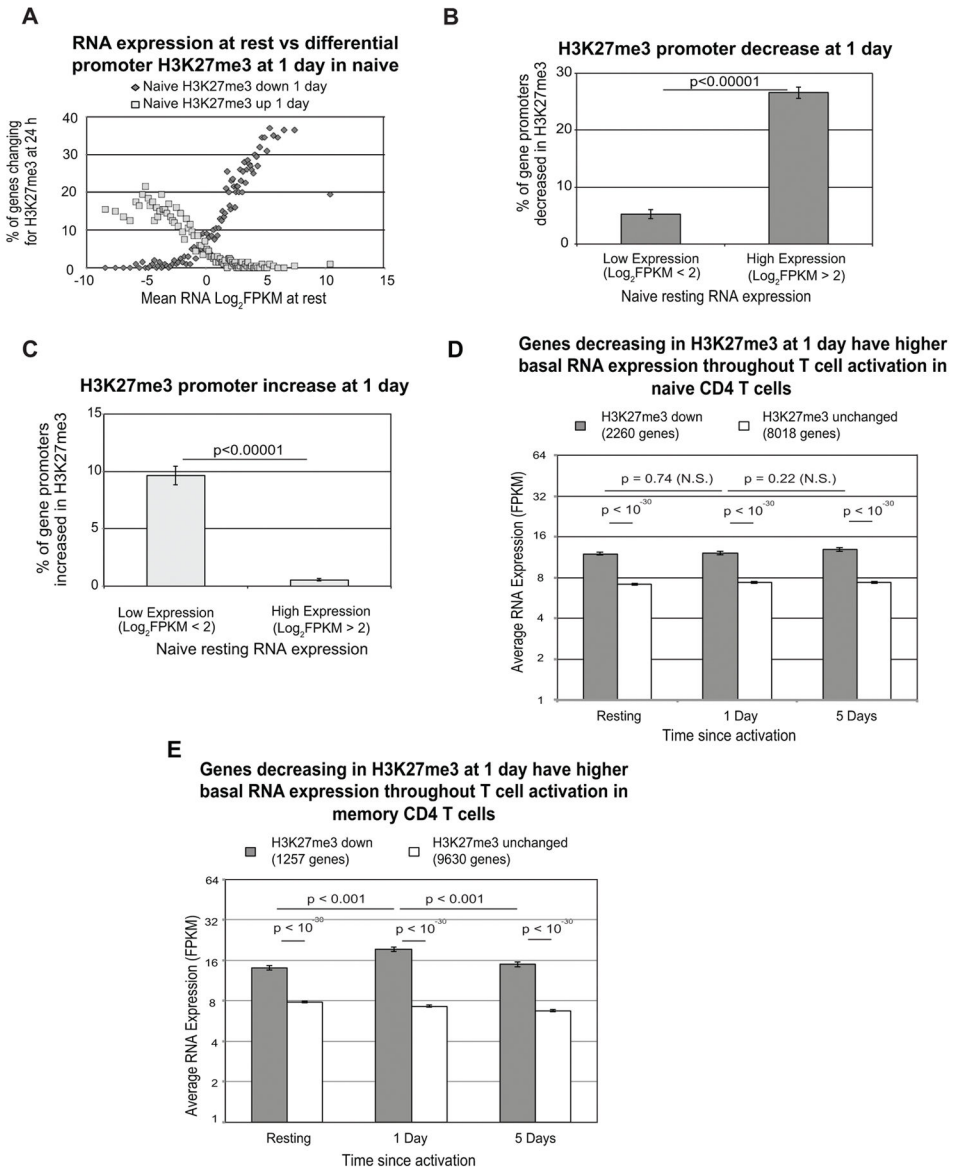

Figure 3. Changes to promoter H3K27me3 during activation maintain baseline expression throughout activation

A) Bins of 200 genes were plotted for RNA expression at rest (x-axis), and the percentage of genes increasing (light gray squares) or decreasing (dark gray diamonds) in promoter H3K27me3 enrichment at 1 day. The percent of genes decreased **(B)** or increased **(C)** in promoter H3K27me3 is significantly different in genes with low vs. high expression in resting naïve CD4 T cells. Error bars represent standard error of the mean. Reported p-value is from two-tailed student T test. **D)** RNA expression for genes decreasing in promoter H3K27me3 after activation is consistently higher throughout CD4 T cell activation than for all other genes with resting RNA expression above 1 FPKM. Error bars represent standard error of the mean. Reported p-values are from one-way ANOVA with Tukey's post hoc analysis. **E)** Repeated analysis for memory CD4 as for naïve in **D)**.

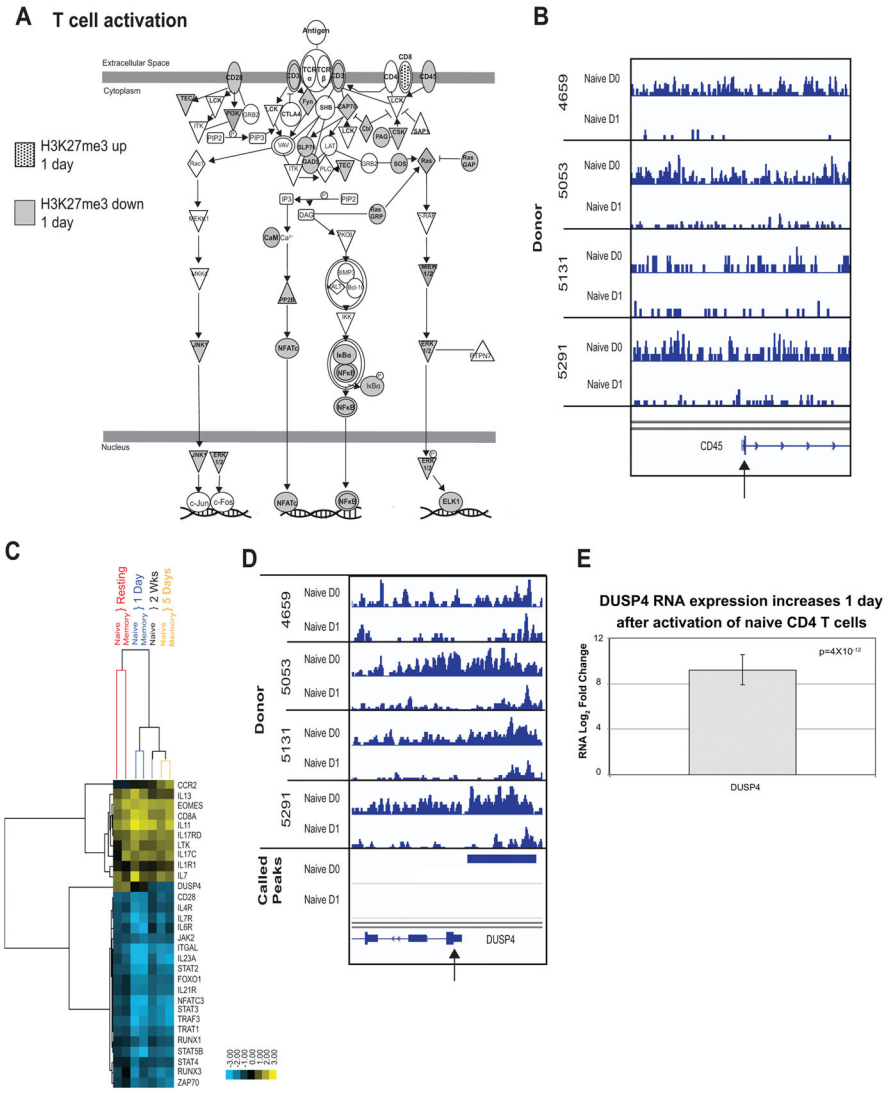

Figure 4. H3K27me3 changes after CD4 T cell activation affect functional pathways important for immune function

A) T cell activation is one of the top pathways affected by promoter H3K27me3 changes 1 day after activation of naïve CD4 T cells. Shaded genes represent genes decreasing in promoter H3K27me3. CD8 is the sole gene increasing in H3K27me3 and is represented by the checked black and white shading. **B)** Genome viewer pileups of H3K27me3 at rest and 1 day activation in naïve cells from 4 donors for CD45, one of the molecules affected by H3K27 demethylation in the activation pathway. **C)** Hierarchical clustering based on H3K27me3 enrichment of 30 selected genes important to immune function that are changing in H3K27me3 during activation reveals that the majority of genes increasing in H3K27me3 begin with high H3K27me3 enrichment at rest (yellow), while those decreasing have low H3K27me3 at rest (blue). **D)** Genome viewer pileups of H3K27me3 at rest and 1 day after activation in naïve cells from 4 donors for DUSP4. The promoter is demarcated by the arrow. A called peak at rest is diminished at 1 day. **E)** DUSP4 RNA expression increases

profoundly 1 day after activation of naïve CD4 T cells. Reported p-value is from edgeR's quasi-likelihood F-test.

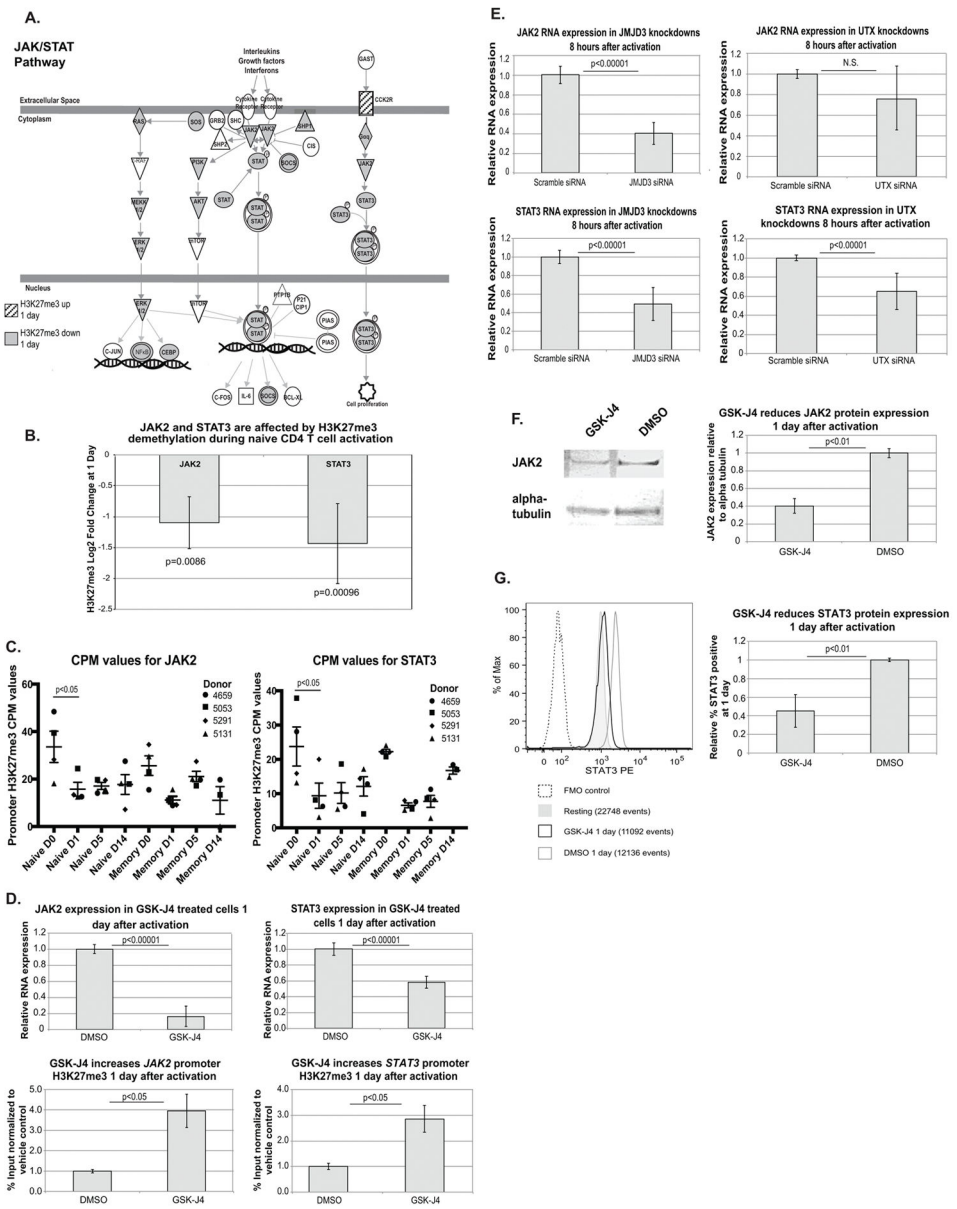

Figure 5. H3K27 demethylation during naïve CD4 T cell activation affects the JAK/STAT pathways

A) Ingenuity Pathway Analysis demonstrates that the JAK/STAT pathway is impacted by changes in H3K27me3 during naïve CD4 T cell activation. Gray shaded genes represent gene promoters losing H3K27me3 at 1 day, while black and white checked genes represent genes gaining H3K27me3 at 1 day. **B)** Differential binding results from ChIP-seq for H3K27me3 of the JAK2 and STAT3 promoter from resting to 1 day after activation in naïve CD4 T cells of 4 healthy donors. Reported p-values are from edgeR's quasi-likelihood F-test. **C)** Counts Per Million (CPM) of H3K27me3 across the JAK2 and STAT3 promoters for all donors across the time course. Horizontal bars represent mean CPM value, while error bars represent standard error of the mean. Reported p-value represents one-tailed student's t-test. **D)** GSK-J4 treatment reduces JAK2 (upper left panel) and STAT3 (upper right panel)

mRNA expression while increasing promoter H3K27me3 of JAK2 (lower left panel) and STAT3 (lower right panel) as measured by quantitative PCR in naïve CD4 T cells from 3 healthy human donors. JAK2 and STAT3 mRNA were measured relative to beta-2 microglobulin and normalized to DMSO vehicle controls. P-values represent one-tailed student's t-test, and error bars in RT-PCR plots represent standard deviation. JAK2 and STAT3 promoter DNA from H3K27me3 ChIPs were measured relative to 2% input controls and normalized to vehicle controls. Reported p-values represent one-tailed student's t-tests, while error bars in ChIP-qPCR plots represent standard error of the mean. **E)** Quantitative RT-PCR of JAK2 and STAT3 in JMJD3 and UTX knockdowns demonstrates that JMJD3 knockdown significantly impacts JAK2 mRNA expression 8 hours after activation of naïve CD4 T cells, while UTX knockdown significantly affects only STAT3 in naïve CD4 T cells of 3 healthy human donors. JAK2 and STAT3 mRNA were measured relative to beta-2 microglobulin and normalized to scramble siRNA controls. Reported p-values represent one-tailed student's t-tests, while error bars represent standard deviation. **F)** Western blotting demonstrates decreased JAK2 expression relative to alpha-tubulin 1 day after activation of naïve CD4 T cells (left panel) with GSK-J4 treatment. Quantitation using densitometry from 3 healthy human subjects demonstrates significantly lower JAK2 protein expression (right panel). Reported p-values represent one-tailed student's t-test. Error bars represent standard deviation. **G)** FACS for STAT3 in GSK-J4 treated naïve CD4 T cells demonstrates decreased protein expression 1 day after activation in 3 healthy human subjects. (Left panel) representative histogram of FACS data from STAT3 stained cells. (Right panel) % of STAT3 positive cells is significantly decreased in GSK-J4 treated cells compared to DMSO vehicle controls in 3 healthy human subjects. Reported p-values represent one-tailed student's t-test. Error bars represent standard error of the mean.

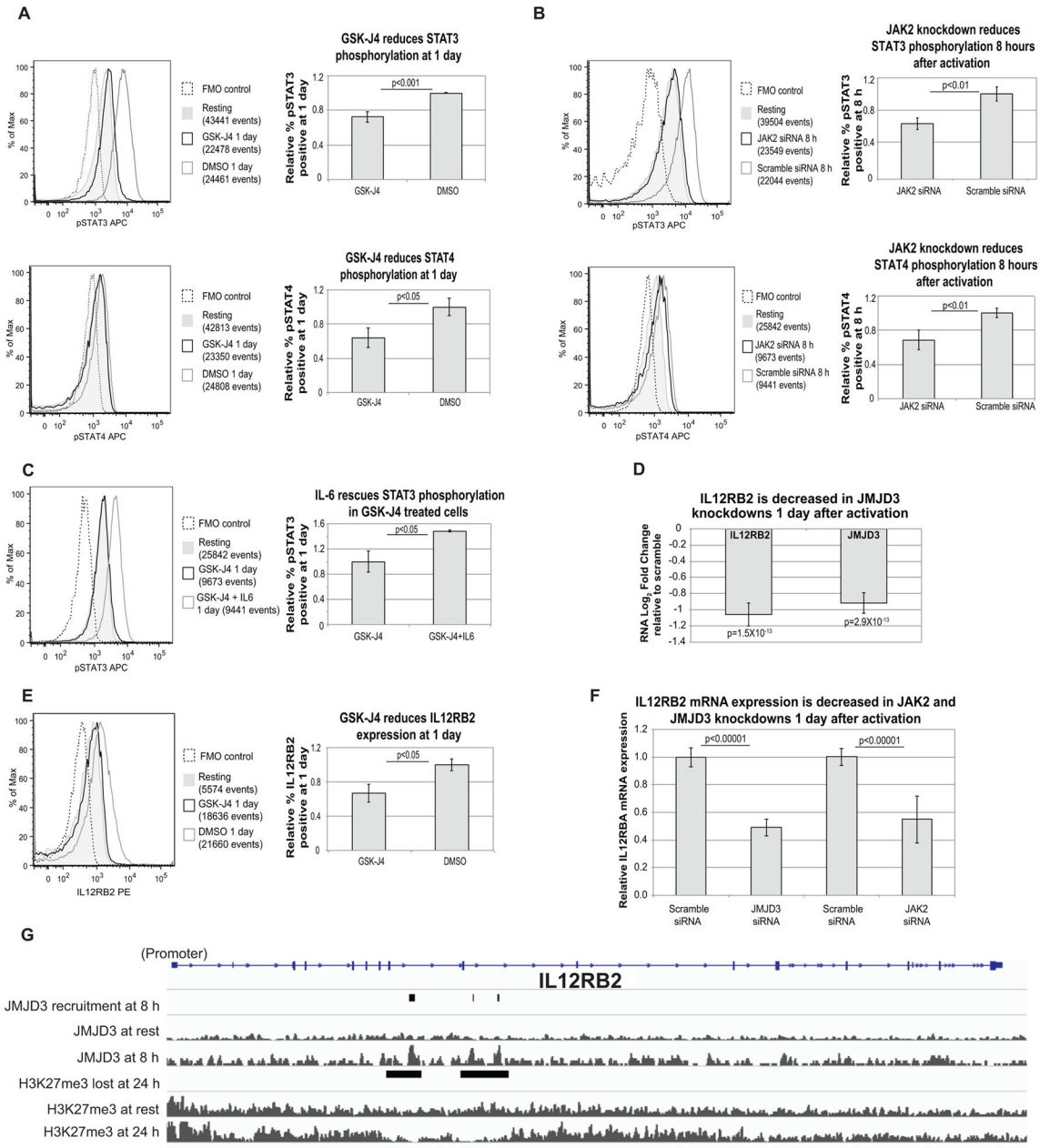

Figure 6. Reduced JAK2 expression associated with loss of H3K27 demethylation during naïve CD4 T cell activation reduces STAT phosphorylation and IL12RB2 expression

A) FACS for pSTAT3 (upper left panel) and pSTAT4 (lower left panel) in GSK-J4 treated cells demonstrates significantly reduced STAT3 and STAT4 phosphorylation relative to DMSO vehicle controls in 3 healthy human subjects (right panels). Reported p-values represent one-tailed student's t-test. Error bars represent standard error of the mean. **B)** FACS for pSTAT3 (upper left panel) and pSTAT4 (lower left panel) of naïve CD4 T cells with JAK2 knockdown demonstrates significantly reduced STAT3 and STAT4 phosphorylation relative to scramble siRNA controls in 3 healthy human subjects (right panels). Reported p-values represent one-tailed student's t-test. Error bars represent standard

error of the mean. **C)** Addition of 20 ng/mL of IL-6 to GSK-J4 treated cells rescues STAT3 phosphorylation after activation of naïve CD4 T cells from 3 healthy human subjects. (Left panel) Representative FACS histogram for pSTAT3. (Right panel) Quantitation of % pSTAT3 positive cells in IL-6 treated cells with GSK-J4 relative to GSK-J4 alone. Reported p-values represent one-tailed student's t-test. Error bars represent standard error of the mean. **D)** RNA-seq of naïve CD4 T cells with JMJD3 knockdown demonstrates reduction in IL12RB2 mRNA relative to the scramble control 1 day after activation in 4 healthy human donors. Reported p-values are from edgeR's quasi-likelihood F-test. **E)** IL12RB2 upregulation is decreased 1 day after activation of GSK-J4-treated naïve CD4 T cells relative to DMSO vehicle controls. (Left panel) Representative FACS histogram for IL12RB2. (Right panel) Quantitation of %IL12RB2 positive cells in GSK-J4 relative to DMSO vehicle controls from 3 healthy human subjects. Reported p-values represent one-tailed student's t-test. Error bars represent standard error of the mean. **F)** Quantitative RT-PCR for IL12RB2 mRNA in naïve CD4 T cells 1 day after activation of JMJD3 and JAK2 knockdowns demonstrates decreased IL12RB2 mRNA expression relative to scramble siRNA controls in 3 healthy human subjects. Reported p-values represent one-tailed student's t-test. Error bars represent standard deviation. **G)** ChIP-seq for JMJD3 8 hours after activation demonstrates peaks within the gene body of IL12RB2 that correspond to the loss of H3K27me3 peaks 1 day after activation. Horizontal bars represent the presence of called peaks.

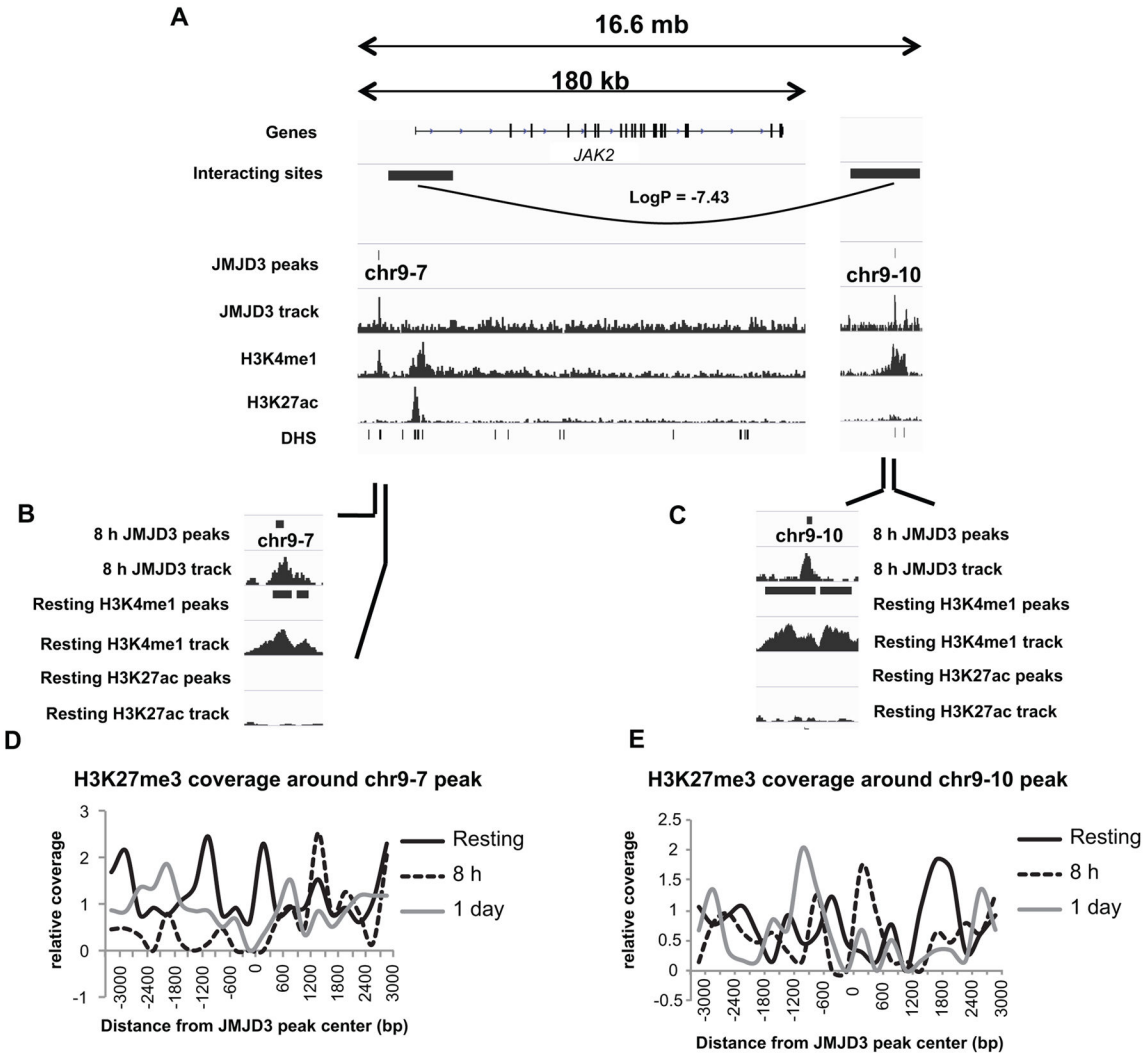

Figure 7. JMJD3 activates distal enhancers of JAK2 by demethylating H3K27me3

(**A**) Promoter-enhancer chromatin interactions identified by HiC in T cells 8 h after activation are overlaid with JMJD3 ChIP-seq at 8 h, as well as H3K4me1 and H3K27ac ChIP-seq in resting naïve CD4 T cells (CD4+CD25−) from ENCODE and DNase hypersensitivity sites in resting naïve CD4 T cells from ENCODE. JMJD3 ChIP-seq peak names are labeled under peak positions. A solid line between promoter and distal interacting sites marks chromatin interactions detected at 8 hours. H3K4me1 and H3K27ac ChIP-seq signals around JMJD3 peak chr9-7 (**B**) and chr9-10 (**C**). H3K27me3 ChIP-seq coverage in CD4 T cells at rest, at 8 h, and at 24 h after activation −/+ 3kb flanking JMJD3 peak centers at chr9-7 (**D**) and chr9-10 (**E**) in the *JAK2* locus.

Table I

Panther pathway analysis reveals the top pathway for genes gaining H3K27me3 promoter peaks 1 day after naïve CD4 T cell activation is WNT signaling. Genes from this subset in the pathway are listed below with their functions.

Entrez ID	Gene Symbol	Gene Name	Function
56100	PCDHGB6	PROTOCADHERIN GAMMA-B6	G-protein coupled receptor
70	ACTC1	ACTIN, ALPHA CARDIAC MUSCLE 1	actin and actin related protein
7474	WNT5A	PROTEIN WNT-5A	signaling molecule
92211	CDHR1	CADHERIN-RELATED FAMILY MEMBER 1	cell junction protein
56131	PCDHB4	PROTOCADHERIN BETA-4	G-protein coupled receptor
5098	PCDHGC3	PROTOCADHERIN GAMMA-C3	G-protein coupled receptor
8325	FZD8	FRIZZLED-8	signaling molecule
1906	EDN1	ENDOTHELIN-1	peptide hormone
2487	FRZB	SECRETED FRIZZLED-RELATED PROTEIN 3	signaling molecule
56122	PCDHB14	PROTOCADHERIN BETA-14	G-protein coupled receptor
9708	PCDHGA8	PROTOCADHERIN GAMMA-A8	G-protein coupled receptor
7477	WNT7B	PROTEIN WNT-7B	signaling molecule
26108	PYGO1	PYGOPUS HOMOLOG 1	transcription cofactor
4854	HDAC3	HISTONE DEACETYLASE 3	reductase
8322	FZD4	FRIZZLED-4	signaling molecule
7483	WNT9A	PROTEIN WNT-9A	signaling molecule
4610	MYCL	PROTEIN L-MYC-RELATED	basic helix-loop-helix transcription factor
85409	NKD2	PROTEIN NAKED CUTICLE HOMOLOG 2	
81029	WNT5B	PROTEIN WNT-5B	signaling molecule
1488	CTBP2	C-TERMINAL-BINDING PROTEIN 2	transcription cofactor
9312	PPP2R5D	SERINE/THREONINE-PROTEIN PHOSPHATASE 2A 56 KDA REGULATORY SUBUNIT DELTA ISOFORM	
56114	PCDHGA1	PROTOCADHERIN GAMMA-A1	G-protein coupled receptor
5099	PCDH7	PROTOCADHERIN-7	cadherin
58	ACTA1	ACTIN, ALPHA SKELETAL MUSCLE	actin and actin related protein
54361	WNT4	PROTEIN WNT-4	signaling molecule
51384	WNT16	PROTEIN WNT-16	signaling molecule
2535	FZD2	FRIZZLED-2	signaling molecule
64072	CDH23	CADHERIN-23	cell junction protein
6934	TCF7L2	TRANSCRIPTION FACTOR 7-LIKE 2	nucleic acid binding
9630	GNA14	GUANINE NUCLEOTIDE-BINDING PROTEIN SUBUNIT ALPHA-14	
8324	FZD7	FRIZZLED-7	signaling molecule
5582	PRKCG	PROTEIN KINASE C GAMMA TYPE	non-receptor serine/threonine protein kinase
3596	FAT2	PROTOCADHERIN FAT 2	

Entrez ID	Gene Symbol	Gene Name	Function
7481	WNT11	PROTEIN WNT-11	signaling molecule
11099	HLTF	HELICASE-LIKE TRANSCRIPTION FACTOR	DNA helicase
57717	PCDHB16	PROTOCADHERIN BETA-16	G-protein coupled receptor
10297	APC2	ADENOMATOUS POLYPOSIS COLI PROTEIN 2	
1004	CDH6	CADHERIN-6	cell junction protein
56129	PCDHB7	PROTOCADHERIN BETA-7	G-protein coupled receptor
9620	CELSR1	CADHERIN EGF LAG SEVEN-PASS G-TYPE RECEPTOR 1	G-protein coupled receptor
7484	WNT9B	PROTEIN WNT-9B	signaling molecule
7471	WNT1	PROTO-ONCOGENE WNT-1	signaling molecule
1000	CDH2	CADHERIN-2	cell junction protein
5100	PCDH8	PROTOCADHERIN-8	G-protein coupled receptor
6424	SFRP4	SECRETED FRIZZLED-RELATED PROTEIN 4	signaling molecule
8641	PCDHGB4	PROTOCADHERIN GAMMA-B4	G-protein coupled receptor
9314	PPP3CA	SERINE/THREONINE-PROTEIN PHOSPHATASE 2B CATALYTIC SUBUNIT ALPHA ISOFORM	protein phosphatase
56135	PCDHAC1	PROTOCADHERIN ALPHA-C1	G-protein coupled receptor
11098	SMARCA2	GLOBAL TRANSCRIPTION ACTIVATOR SNF2L2-RELATED	DNA helicase
83999	KREMEN1	KREMEN PROTEIN 1	receptor
79633	FAT4	PROTOCADHERIN FAT 4	
2494	CTBP1	C-TERMINAL-BINDING PROTEIN 1	transcription cofactor
2786	GNG4	GUANINE NUCLEOTIDE-BINDING PROTEIN G(I)/G(S)/G(O) SUBUNIT GAMMA-4	ortholog
8714	PCDHGB7	PROTOCADHERIN GAMMA-B7	G-protein coupled receptor
6697	LRP5	LOW-DENSITY LIPOPROTEIN RECEPTOR-RELATED PROTEIN 5	receptor
57575	PCDH10	PROTOCADHERIN-10	G-protein coupled receptor
7480	WNT10B	PROTEIN WNT-10B	signaling molecule
127602	MYCLP1	PROTEIN L-MYC-RELATED	basic helix-loop-helix transcription factor
56098	PCDHGC4	PROTOCADHERIN GAMMA-C4	G-protein coupled receptor
57526	PCDH19	PROTOCADHERIN-19	cadherin
4613	MYCN	N-MYC PROTO-ONCOGENE PROTEIN	basic helix-loop-helix transcription factor
4036	LRP2	LOW-DENSITY LIPOPROTEIN RECEPTOR-RELATED PROTEIN 2	receptor
2195	FAT1	PROTOCADHERIN FAT 1	
6862	T	BRACHYURY PROTEIN	transcription factor
999	CDH1	CADHERIN-1	cell junction protein
7088	TLE1	TRANSDUCIN-LIKE ENHANCER PROTEIN 1	transcription cofactor
56105	PCDHGA11	PROTOCADHERIN GAMMA-A11	G-protein coupled receptor
7473	WNT3	PROTO-ONCOGENE WNT-3	signaling molecule
3084	DVL1	SEGMENT POLARITY PROTEIN DISHEVELLED HOMOLOG DVL-1-RELATED	signaling molecule

Table II

Ingenuity Pathway Analysis reveals the top pathway for promoters increasing in H3K27me3 1 day after activation of naïve CD4 T cells is embryonic stem cell pluripotency.

Entrez Gene	Symbol	Entrez Gene Name	Function
627	BDNF	brain-derived neurotrophic factor	growth factor
650	BMP2	bone morphogenetic protein 2	growth factor
652	BMP4	bone morphogenetic protein 4	growth factor
654	BMP6	bone morphogenetic protein 6	growth factor
353500	BMP8A	bone morphogenetic protein 8a	cytokine
656	BMP8B	bone morphogenetic protein 8b	growth factor
2260	FGFR1	fibroblast growth factor receptor 1	kinase
2535	FZD2	frizzled class receptor 2	G-protein coupled receptor
7855	FZD5	frizzled class receptor 5	G-protein coupled receptor
8324	FZD7	frizzled class receptor 7	G-protein coupled receptor
8325	FZD8	frizzled class receptor 8	G-protein coupled receptor
2778	GNAS	GNAS complex locus	enzyme
3624	INHBA	inhibin, beta A	growth factor
22808	MRAS	muscle RAS oncogene homolog	enzyme
4838	NODAL	nodal growth differentiation factor	growth factor
4909	NTF4	neurotrophin 4	growth factor
4914	NTRK1	neurotrophic tyrosine kinase, receptor, type 1	kinase
4916	NTRK3	neurotrophic tyrosine kinase, receptor, type 3	kinase
5155	PDGFB	platelet-derived growth factor beta polypeptide	growth factor
5156	PDGFRA	platelet-derived growth factor receptor, alpha polypeptide	kinase
53637	S1PR5	sphingosine-1-phosphate receptor 5	G-protein coupled receptor
57167	SALL4	spalt-like transcription factor 4	transcription regulator
83439	TCF7L1	transcription factor 7-like 1 (T-cell specific, HMG-box)	transcription regulator
8433	UTF1	undifferentiated embryonic cell transcription factor 1	transcription regulator
7473	WNT3	wingless-type MMTV integration site family, member 3	other
54361	WNT4	wingless-type MMTV integration site family, member 4	cytokine
7475	WNT6	wingless-type MMTV integration site family, member 6	other
7481	WNT11	wingless-type MMTV integration site family, member 11	other
80326	WNT10A	wingless-type MMTV integration site family, member 10A	other
7480	WNT10B	wingless-type MMTV integration site family, member 10B	other
7482	WNT2B	wingless-type MMTV integration site family, member 2B	other
7474	WNT5A	wingless-type MMTV integration site family, member 5A	cytokine
81029	WNT5B	wingless-type MMTV integration site family, member 5B	other
7477	WNT7B	wingless-type MMTV integration site family, member 7B	other
7484	WNT9B	wingless-type MMTV integration site family, member 9B	other

Table III

Canonical pathways for genes decreased in promoter H3K27me3 1 day after activation of naïve CD4 T cells.

Ingenuity Canonical Pathways	−log(p-value)
Protein Ubiquitination Pathway	7.3
IGF-1 Signaling	5.6
Glucocorticoid Receptor Signaling	5.5
T Cell Receptor Signaling	5.5
Integrin Signaling	5.4
Erythropoietin Signaling	5.3
JAK/Stat Signaling	4.7
HGF Signaling	4.7
Insulin Receptor Signaling	4.7
NF-κB Signaling	4.7
FLT3 Signaling in Hematopoietic Progenitor Cells	4.6
ERK/MAPK Signaling	4.5
Myc Mediated Apoptosis Signaling	3.9
IL-3 Signaling	3.9
RAR Activation	3.9
SAPK/JNK Signaling	3.8
Regulation of IL-2 Expression in Activated and Anergic T Lymphocytes	3.8
Regulation of eIF4 and p70S6K Signaling	3.7
FAK Signaling	3.7
TGF-β Signaling	3.7
Glioma Signaling	3.7
14-3-3-mediated Signaling	3.6
Growth Hormone Signaling	3.6
Antiproliferative Role of TOB in T Cell Signaling	3.5
Telomerase Signaling	3.5
ErbB Signaling	3.4
EIF2 Signaling	3.3
Virus Entry via Endocytic Pathways	3.2
NF-κB Activation by Viruses	3.2
Lymphotoxin β Receptor Signaling	3.2
IL-2 Signaling	3.2
Rac Signaling	3.1
CTLA4 Signaling in Cytotoxic T Lymphocytes	3.0